

Multifunctional Redox-Tuned Viologen-Based Covalent Organic Polymers

Gobinda Das,^{#a} Thirumurugan Prakasam,^{#a} Selbi Nuryyeva,^a Dong Suk Han,^b Ahmed Abdel-Wahab,^b John-Carl Olsen^c, Kyriaki Polychronopoulou,^d Carlos Platas-Iglesias,^e Florent Ravoux,^f Mustapha Jouiad,^f and Ali Trabolsi^{a*}

^a New York University Abu Dhabi (NYUAD), Experimental Research Building (C1), Saadiyat Island, Abu Dhabi, United Arab Emirates. E-mail: ali.trabolsi@nyu.edu

^b Chemical Engineering Program, Texas A&M University at Qatar, Education City, Doha, Qatar

^c School of Sciences, Indiana University Kokomo, Kokomo, IN 46904, USA

^d Mechanical Engineering Department, Khalifa University of Science, Technology and Research, Abu Dhabi, P.O. Box 127788, UAE

^e Departamento de Química Fundamental, Universidade da Coruña, Campus da Zapateira, Rúa da Fraga 10, 15008 A Coruna, Spain.

Supporting Information

Table of Contents

- General materials and methods**
- S1: Synthetic strategy employed in the preparation of the polymers (COP₁⁺⁺ and COP₂⁺⁺) and their starting materials**
- S2: Fourier Transform Infrared (FTIR) Spectroscopy**
- S3: TG analyses of the polymers in their different redox states**
- S4: Solid state CP/MAS ¹³C NMR spectra of COP₁⁺⁺ and COP₂⁺⁺**
- S5: Solid state ³¹P spectra of COP₁⁺⁺ and COP₂⁺⁺**
- S6: PXRD analyses of the polymers in their different redox states**
- S7: Stability test of the polymers in ethanol.**
- S8: HRTEM images of the polymers COP₁⁺⁺ and COP₂⁺⁺.**
- S9: Solid state EPR analysis of the polymer (COP₂⁺⁺, COP₂^{•+} and COP₂⁰)**
- S10: Radical stability of the polymer COP₁^{•+} over time**
- S11: SEM analysis after exposure to sunlight**
- S12: UV-Vis spectroscopic measurements for all polymers**
- S13: Stability the polymers during ammonia detection**
- S14: Nitrogen (N₂) and carbon dioxide (CO₂) adsorption study for COP₁⁺⁺ and COP₂⁺⁺**
- S15: UV/Vis spectral study of free iodine at different concentration.**
- S16: Time-dependent removal efficiency of iodine**
- S17: Theoretical study of polymers to understand the mechanism for iodine and ammonia capture**
- S18: Solid state Raman spectral analysis of all iodine loaded polymers**
- S19: Solid state XPS analysis of all the iodine loaded polymers**
- S20: Comparison of iodine capture with other reported materials**
- S21: Energy-dispersive X-ray spectroscopy study**
- S22: Characterization of polymer after iodine removal**
- S23: Reusability study of the polymers after iodine and dichromate removal**

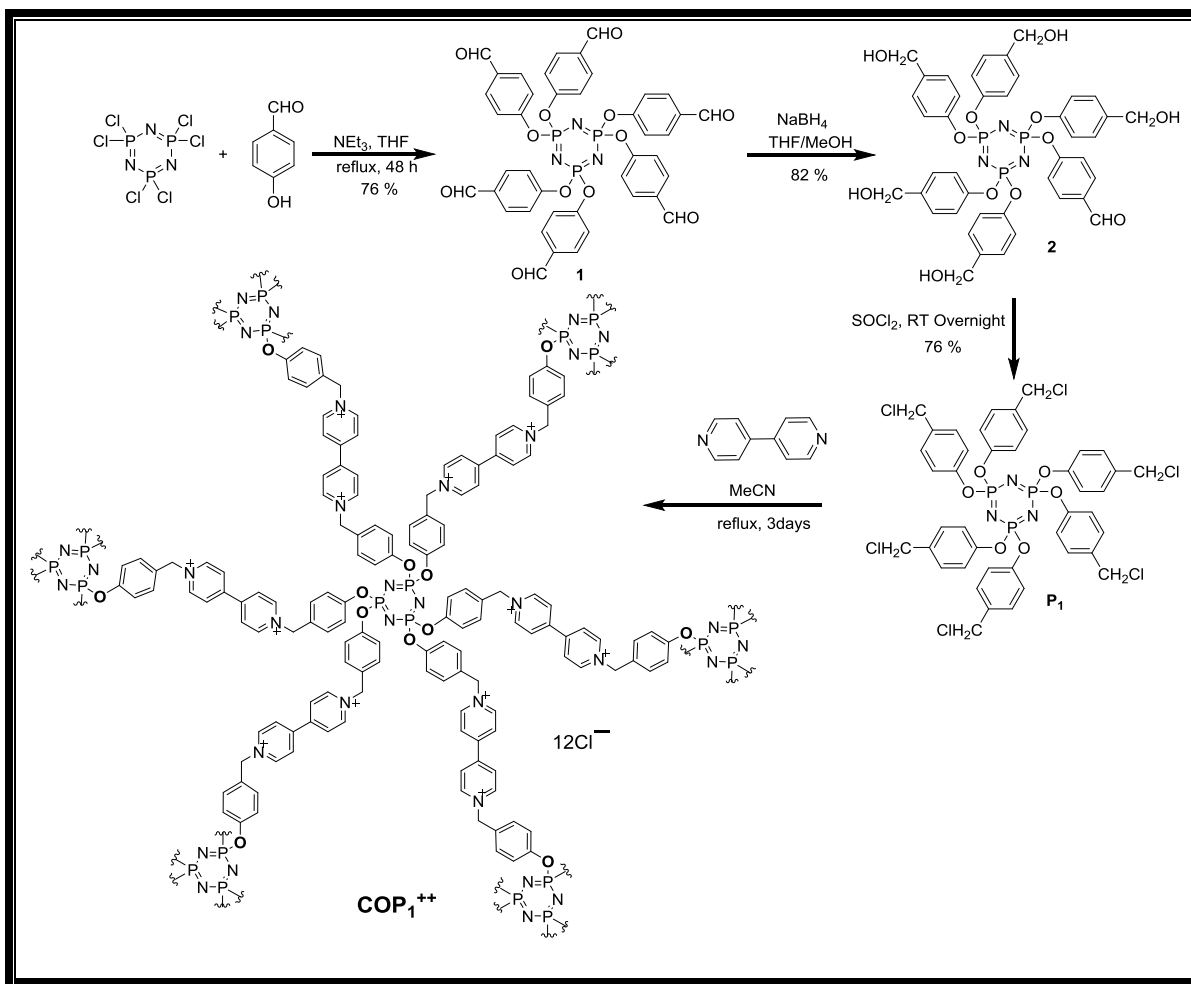
1. General Materials and Methods

All reagents and starting materials were purchased from Sigma-Aldrich and used without further purification. Syntheses of precursors 1,1'-bis(2,4-dinitrophenyl)dichloride, 4,4'-bipyridinium, (DNP-BP), hexakis(4-chloromethylphenoxy)cyclotriphosphazene (**P**₁), and hexakis(4-aminophenoxy)cyclotriphosphazene (**P**₂) were accomplished according to the literature^{1,2,3} with slight modification and are reported in the synthesis section. Deionized water was used from Millipore Gradient Milli-Q water purification system. Thin-layer chromatography (TLC) was performed on silica gel 60 F254 (E. Merck). The plates were inspected with UV light. Column chromatography was performed on silica gel 60F (Merck 9385, 0.040–0.063 mm). Routine nuclear magnetic resonance (NMR) spectra were recorded at 25 °C on a Bruker Avance spectrometer, with working frequency of 600 and 500 MHz for ¹H, and 151.0 MHz for ¹³C nuclei, respectively. All chemical shifts are reported in ppm relative to the signals corresponding to the residual non-deuterated solvents (CD₃CN: δ = 1.94 ppm, CD₃OD: δ = 3.31 ppm, D₂O: δ = 4.97 ppm and DMSO-d₆: δ = 2.50 ppm). Coupling constant values (*J*) are given in hertz (Hz), the multiplicity is abbreviated in the following way: s (singlet) and d (doublet). FTIR studies were carried out on Agilent 670-IR spectrometer. TGA experiments were performed on TA SDT Q600. SEM images were obtained from FEI Quanta 450FEG. UV-Vis studies were carried out on Cary 5000 UV-Vis-NIR spectrophotometer. All UV-Vis spectra were recorded at room temperature of 298 K in a quartz cell with 10 mm path length. Solid-state crosspolarization magic angle spinning (CP/MAS) ¹³C and ³¹P NMR spectra of polymers were recorded on a Bruker Avance III 400 WB (400 MHz) NMR spectrometer at ambient temperature with a magic angle spinning rate of 7.0 kHz. Raman measurements were performed with a Witec Alpha 300 confocal Raman system. The samples were illuminated with a 532 nm laser and an acquisition

times between 25 and 80 s. CO₂ and N₂ adsorption/desorption isothermal curves were recorded both at 273 K and 298 K and up to 1 bar using a manometric Micromeritics 3Flex gas sorption analyzer along with a PolyScience Circulating bath (50:50 vol% water:ethylene glycol mixture) for maintaining constant temperature during experiment.

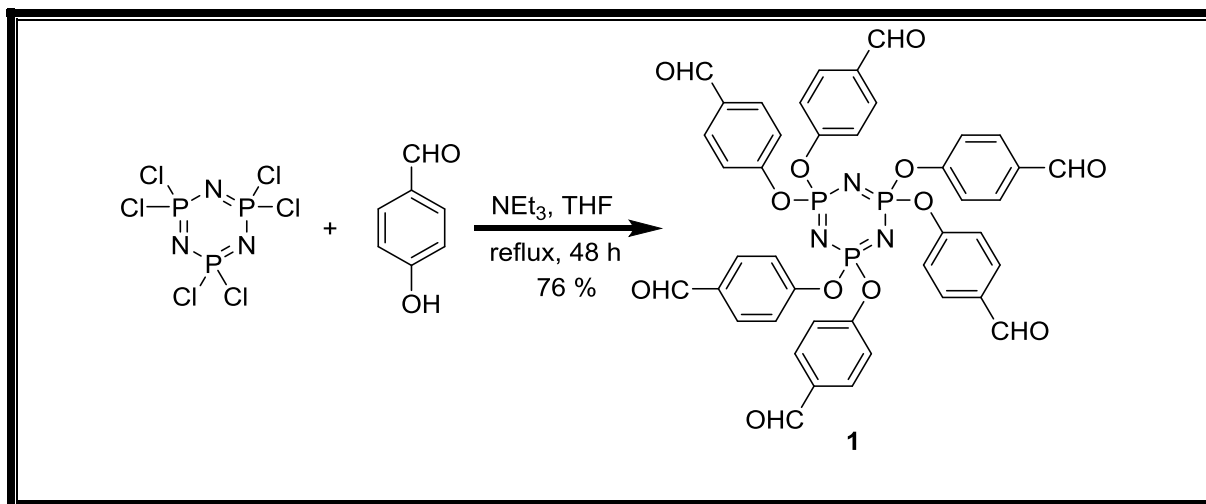
S1: Synthesis of the polymers (COP₁⁺⁺ and COP₂⁺⁺)

Synthetic strategy employed in the preparation of the polymer (COP₁⁺⁺)



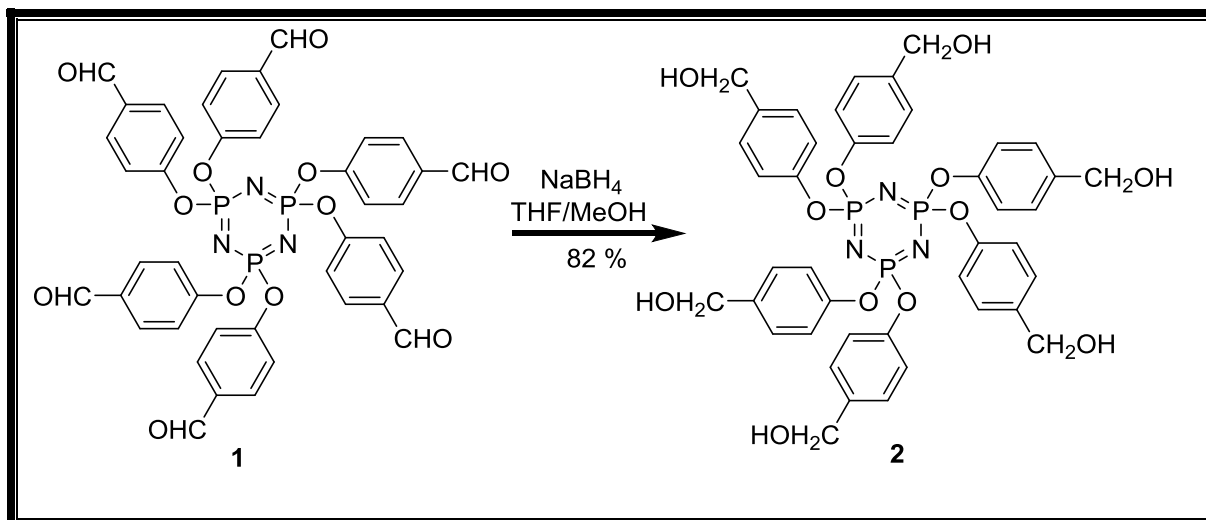
Scheme 1. Synthetic route for the preparation of COP₁⁺⁺ polymer starting from phosphonitrilic chloride trimer and 4-hydroxybenzaldehyde.

a) Synthesis of hexakis(4-formylphenoxy)cyclotriphosphazene



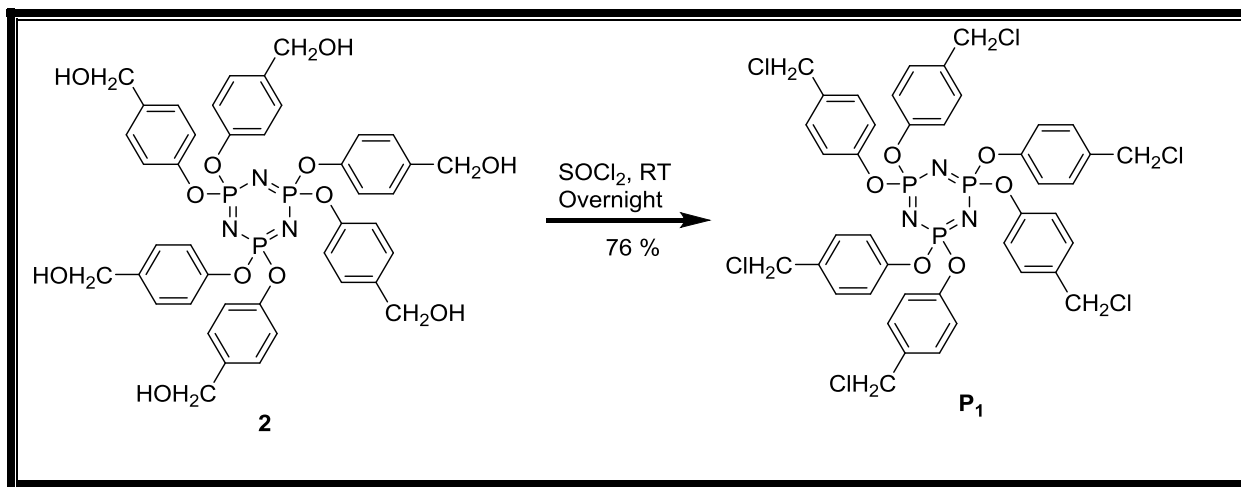
Compound (**1**) was synthesized according to a previous synthetic report with minor modifications.² *p*-hydroxybenzaldehyde (11.1 g, 0.091 mol) was added to a solution of phosphonitrilic chloride trimer (5.1 g, 0.015 mol) and triethylamine (12.0 g, 0.119 mol) in 20 mL THF. The reaction mixture was refluxed for 48 hours. After completion of the reaction, the mixture was cooled to room temperature and filtered. The filtrate was concentrated under reduced pressure. The concentrated residue was then recrystallized from ethyl acetate yielding a yellow powder of **1** (9.6 g, 76% yield). ^1H NMR (500 MHz, CDCl_3) δ : 9.86 (s, 6H, Ar-CHO), 7.67 (d, $J = 7.5$ Hz, 12 H, Ar-H), 7.08 (d, $J = 7.5$ Hz, 12 H, Ar-H); ^{31}P NMR (202.404 MHz, CDCl_3) δ : 7.07; ^{13}C NMR (125 MHz, CDCl_3) δ : 190.4, 146.1, 141.2, 121.4, 114.5.

b) Synthesis of hexakis(4-hydroxymethylphenoxy)cyclotriphosphazene



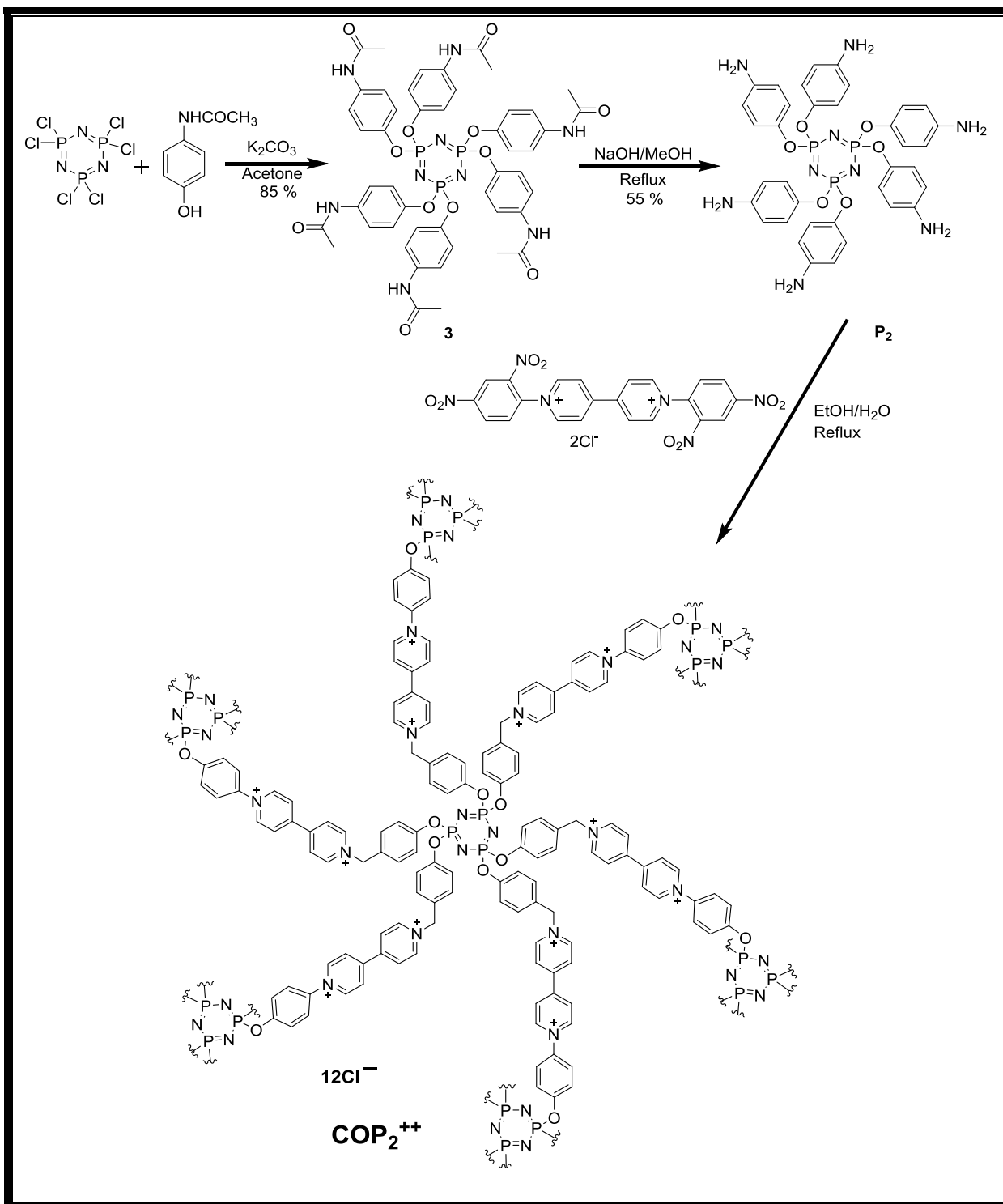
Compound **2** was synthesized according to the literature with minor modifications.² Sodium borohydride (4.0 g, 0.11 mol) was added to a solution of **1** (9.6 g, 0.011 mol) in 200 mL THF/MeOH (1:1 ratio), and the mixture was stirred at room temperature overnight. The solvent was removed under reduced pressure. To the residue, 200 mL of deionized H_2O was added, and then the precipitate was collected by filtration and recrystallized from methanol to yield **2** as a white powder (8.0 g, 82% yield). ^1H NMR (500 MHz, CDCl_3) δ : 7.21 (d, $J = 8.5$ Hz, 12H, Ar-*H*), 6.81 (d, $J = 8.0$ Hz, 12H, Ar-*H*), 5.25 (s, 6H, -OH), 4.48 (s, 12H, -Ar- CH_2); ^{31}P NMR (202.404 MHz, CDCl_3) δ : 8.86; ^{13}C NMR (125 MHz, CDCl_3) δ : 149.3, 139.8, 128.6, 120.6, 62.9.

c) Synthesis of hexakis(4-chloromethylphenoxy)cyclotriphosphazene



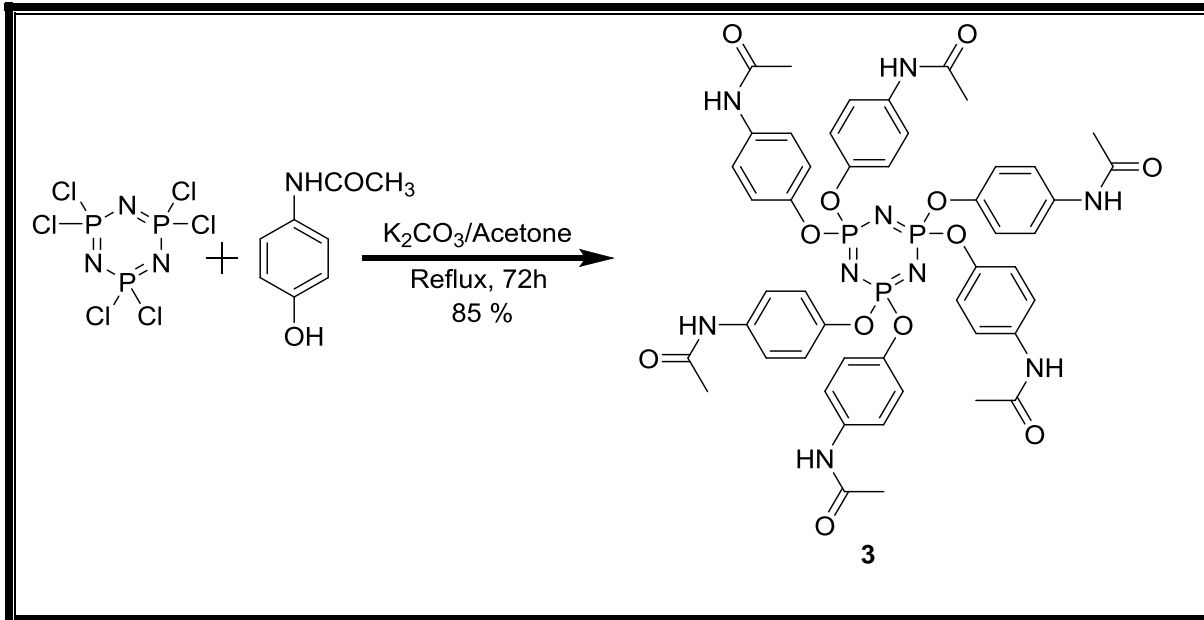
Compound **2** (8.0 g, 0.009 mol) was chloromethylated with thionyl chloride, SOCl₂ (147.6 g, 1.24 mol). The reaction was left to stir at room temperature overnight. Thionyl chloride was then removed under reduced pressure and the crude product was recrystallized from chloroform resulting in white crystalline compound of **P₁** (6.9 g, 76% yield). ¹H NMR (500 MHz, CDCl₃) δ: 7.34 (d, *J* = 8.5 Hz, 12H, Ar-*H*), 6.87 (d, *J* = 8.5 Hz, 12H, Ar-*H*), 4.76 (s, 12H, -Ar-CH₂); ³¹P NMR (202.404 MHz, CDCl₃) δ: 8.76; ¹³C NMR (125 MHz, CDCl₃) δ: 150.2, 134.3, 129.7, 121.2, 45.6.

Synthetic strategy employed in the preparation of the polymer (COP_2^{++})



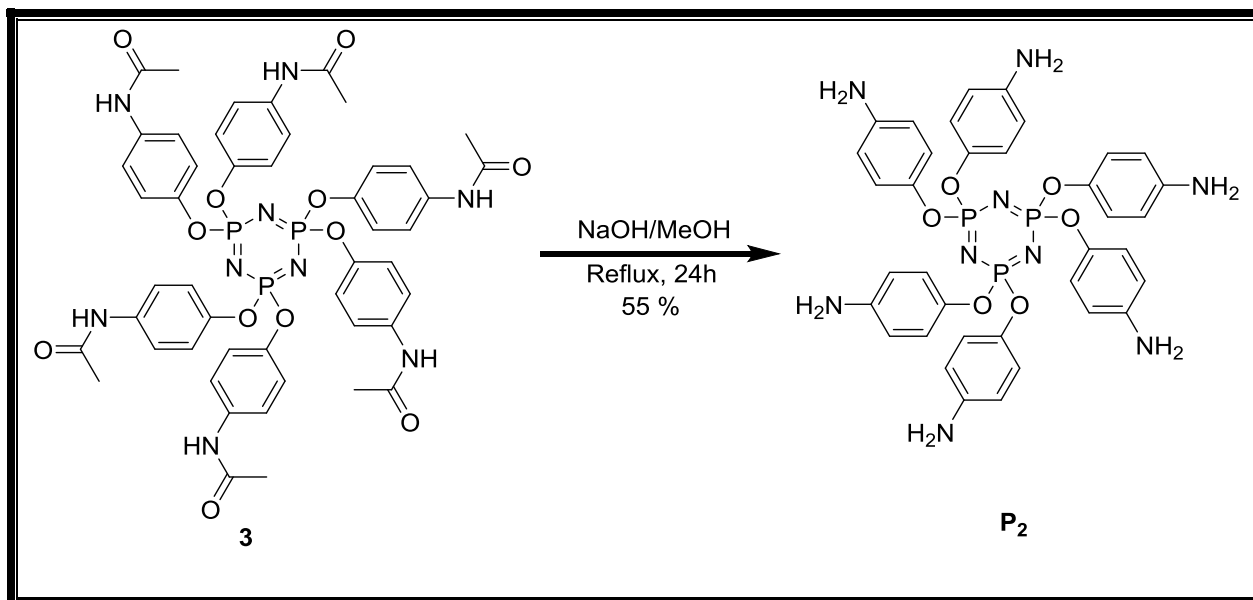
Scheme 2. Synthetic route for the preparation of COP_2^{++} from phosphonitrilic chloride trimer and N-(4-hydroxyphenyl)acetamide.

a) Synthesis of hexakis(4-acetamidophenoxy)cyclotriphosphazene



To a solution of phosphonitrilic trimer (2.04 g, 0.006 mol) in 200 mL of acetone, N-(4-hydroxyphenyl)acetamide (7.4 g, 0.048 mol) and potassium carbonate (9.6 g, 0.072 mol) were added. The reaction was refluxed for 72 hours. The solution was cooled down to room temperature. The precipitate was filtered and thoroughly washed with water (2×60 mL) and ethanol (2×30 mL). The product was then dried under vacuum to give (**3**) as a white powder, (2.6 g, 85% yield). 1H NMR (500 MHz, DMSO) δ : 9.95 (s, 6H, N-H), 7.45 (d, J = 8.5 Hz, 12H, Ar-H), 6.81 (d, J = 8.5 Hz, 12H, Ar-H), 2.51 (s, 18H, $-COCH_3$); ^{31}P NMR (202.404 MHz, DMSO) δ : 9.18.

b) Synthesis of hexakis(4-aminophenoxy)cyclotriphosphazene



To a solution of **3** (1.57 g, 1.5 mmol) in 80 mL methanol, sodium hydroxide solution (7.4 g, 17 M) in water was added. The reaction was refluxed for 24 hours. The precipitate was filtered out from the hot solution and the filtrate was left to recrystallize. Resulting crystals were filtered out, washed with ethanol and diethyl ether to give **P₂** as a light pink powder (0.7 g, 55% yield). ¹H NMR (500 MHz, DMSO) δ : 6.51 (d, $J = 9$ Hz, 12H, Ar-*H*), 6.43 (d, $J = 9$ Hz, 12H, Ar-*H*), 4.90 (s, 12H, -NH₂) ³¹P NMR (202.404 MHz, DMSO) δ : 10.02; ¹³C NMR (125 MHz, DMSO) δ : 114.7, 121.4, 141.3, 146.1.

S2. Fourier Transform Infrared (FTIR) Spectroscopy

The formation of the two polymers (COP₁⁺⁺ and COP₂⁺⁺) was confirmed and elucidated by FTIR using an Agilent Technologies Cary 600 Series FTIR Spectrometer. The following figures (Figure S1 and Figure S2) display the characteristic absorption bands of the polymers and the starting materials.

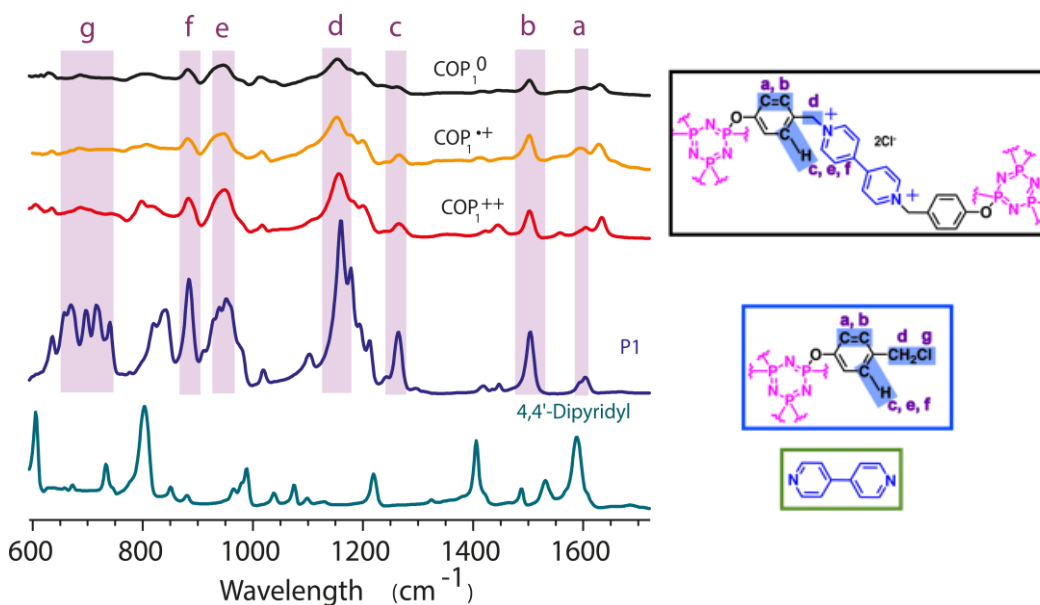


Figure S1: FTIR spectra of the three redox states of viologen polymers COP_1^{0} , COP_1^{+} and COP_1^{2+} stacked with the two precursor materials 4,4'-bipyridine and hexakis(4-chloromethylphenoxy)cyclotriphosphazene (**P1**).

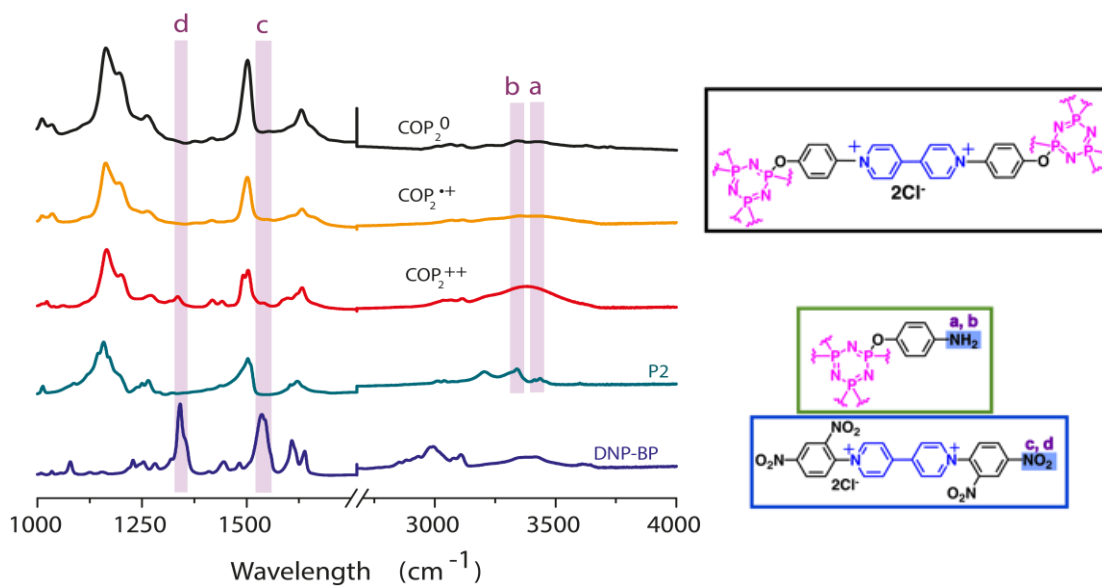


Figure S2: FTIR spectra of the three redox states of viologen polymers namely COP_2^{0} , COP_2^{+} and COP_2^{2+} stacked with their precursors hexakis(4-aminophenoxy)cyclotriphosphazene and 4,4'-bipyridinium, 1,1'-bis(2,4-dinitrophenyl)dichloride (**P2**).

S3: Thermogravimetric analyses of the polymers in their different oxidation states. The figures S₃-S_{8a} display the thermal stability of all six polymers studied in this work.

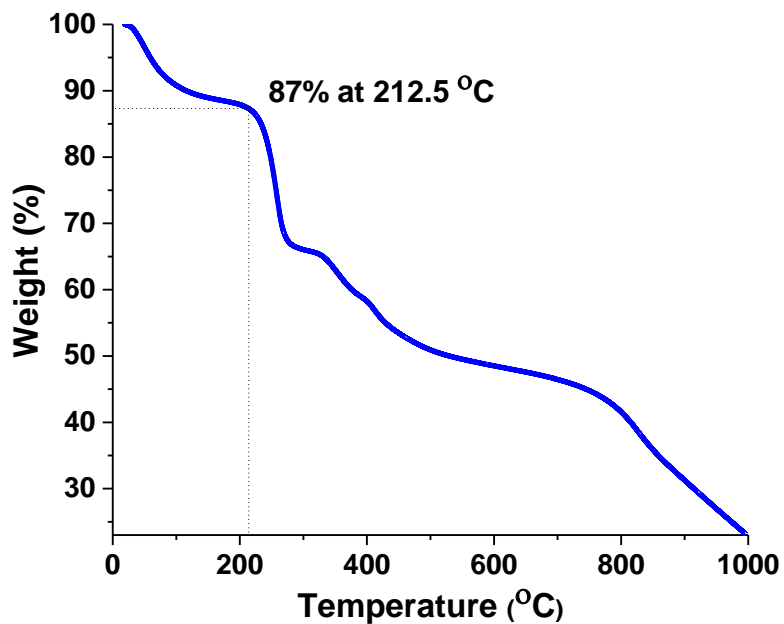


Figure S3: TGA profile for COP₁⁺⁺.

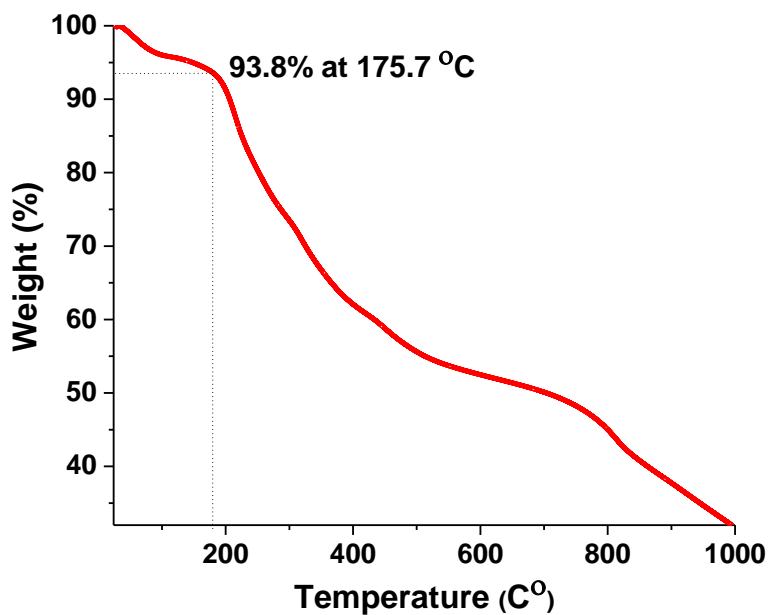


Figure S4: TGA profile for COP₁^{*+}.

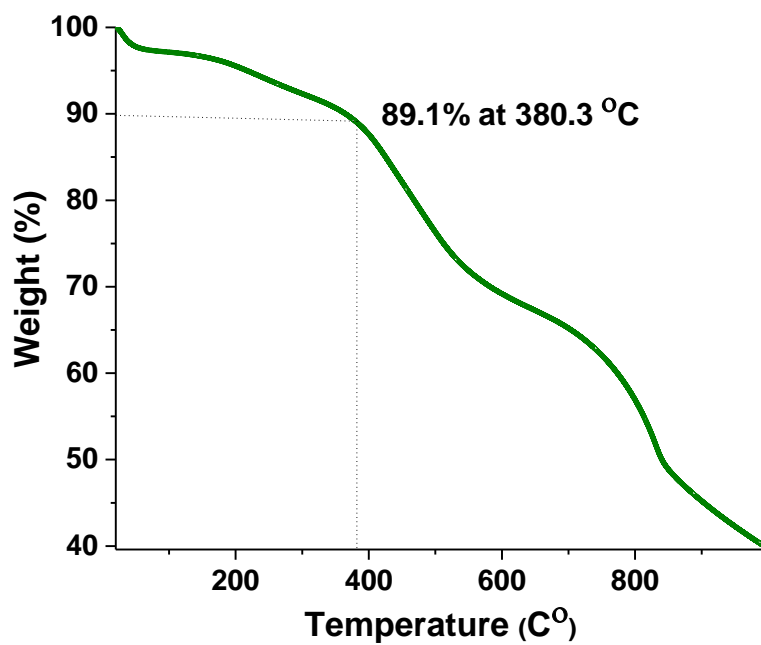


Figure S5: TGA profile for COP₁⁰.

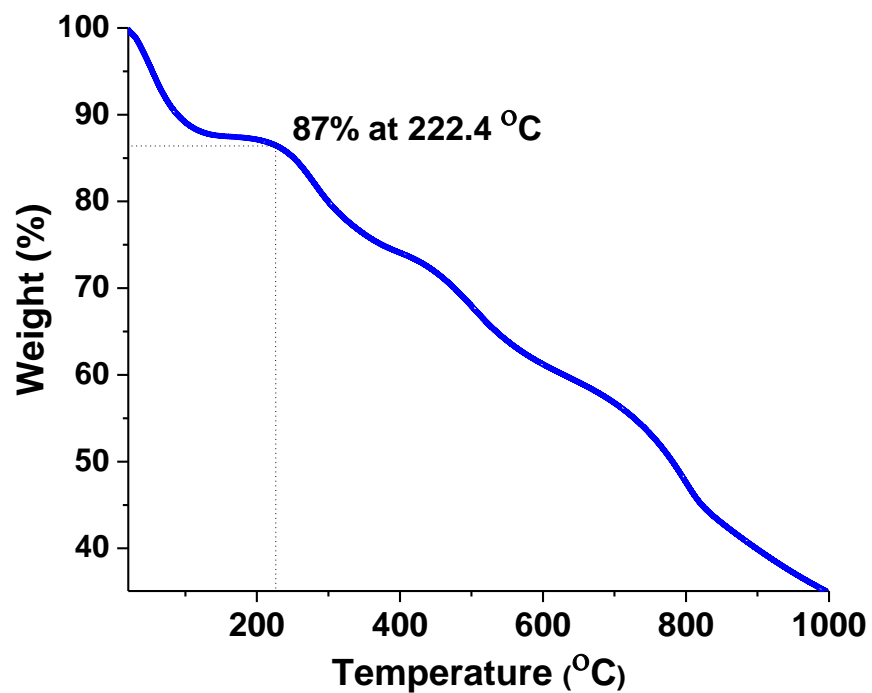


Figure S6: TGA profile for COP₂⁺⁺.

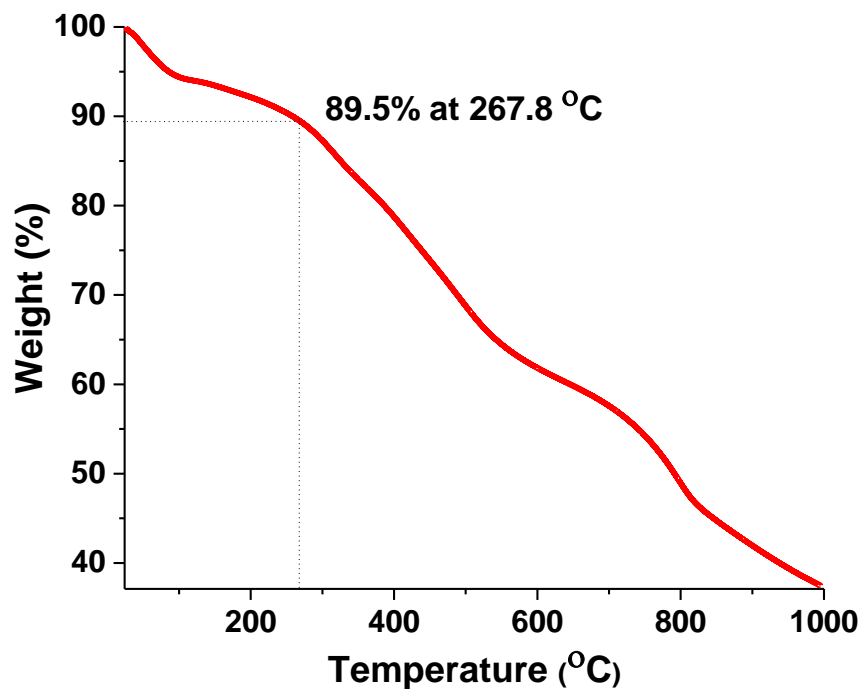


Figure S7: TGA profile for COP₂*+.

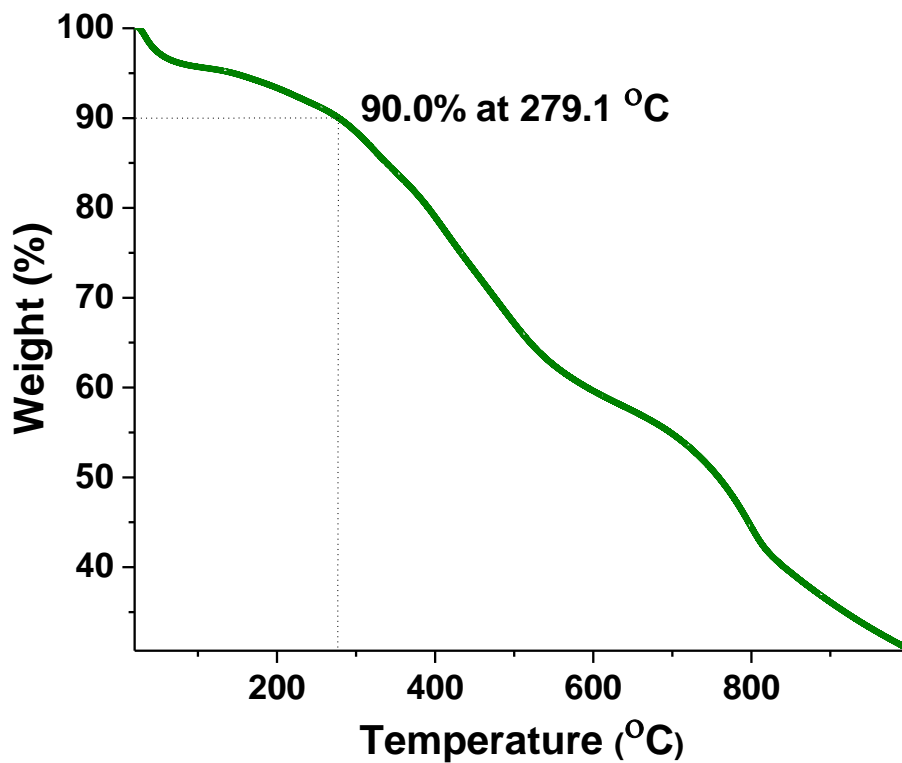


Figure S8: TGA profile for COP₂⁰.

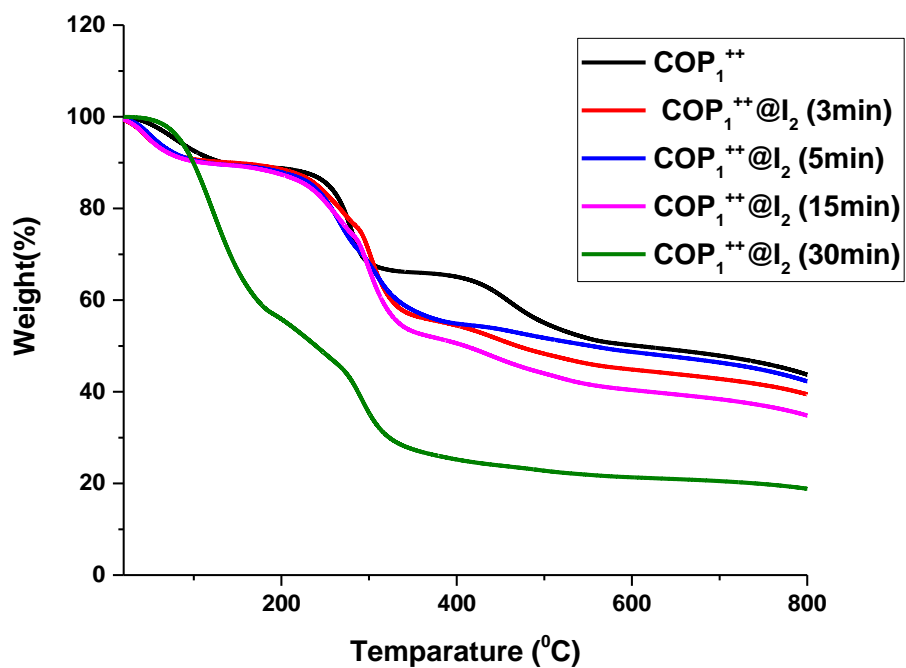


Figure S8a: TGA profile for $\text{COP}_1^{++}@I_2$ at different time intervals.

S4: Solid state CP/MAS ^{13}C NMR spectra of COP_1^{++} and COP_2^{++}

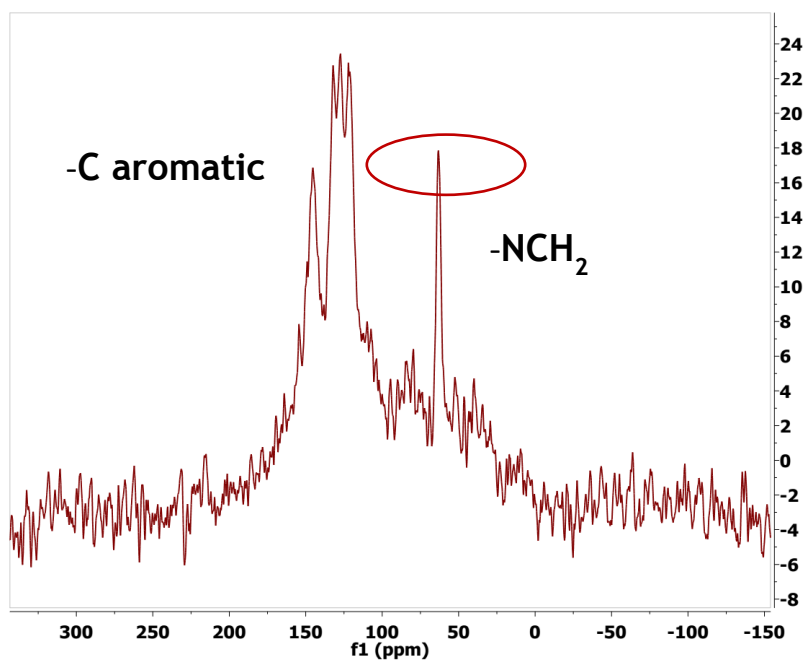


Figure S9: CP/MAS ^{13}C NMR spectrum of COP_1^{++} and the corresponding peak assignments.

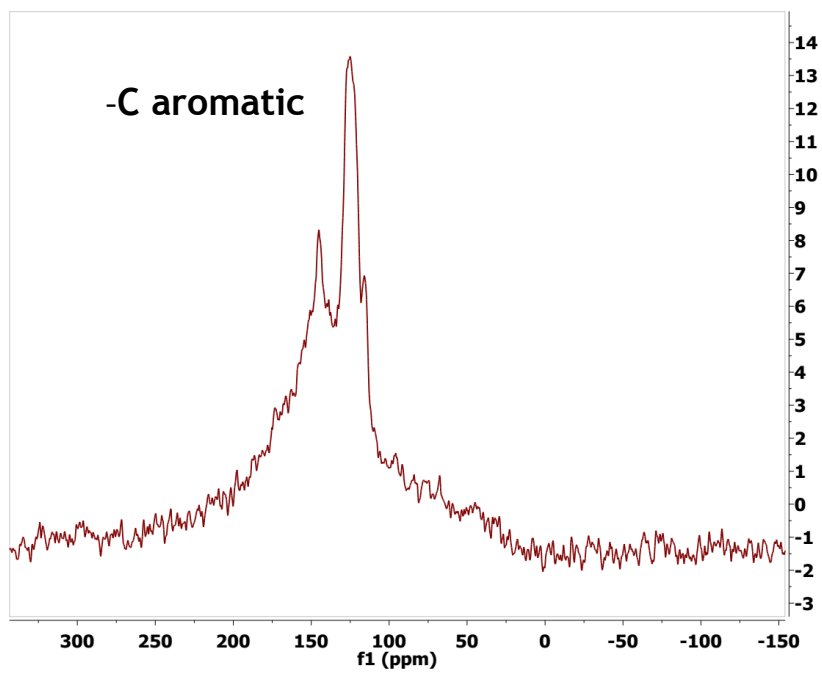


Figure S10: CP/MAS ^{13}C NMR spectrum of COP_2^{++} and the corresponding peak assignment.

S5: Solid state ^{31}P spectra of COP_1^{++} and COP_2^{++}

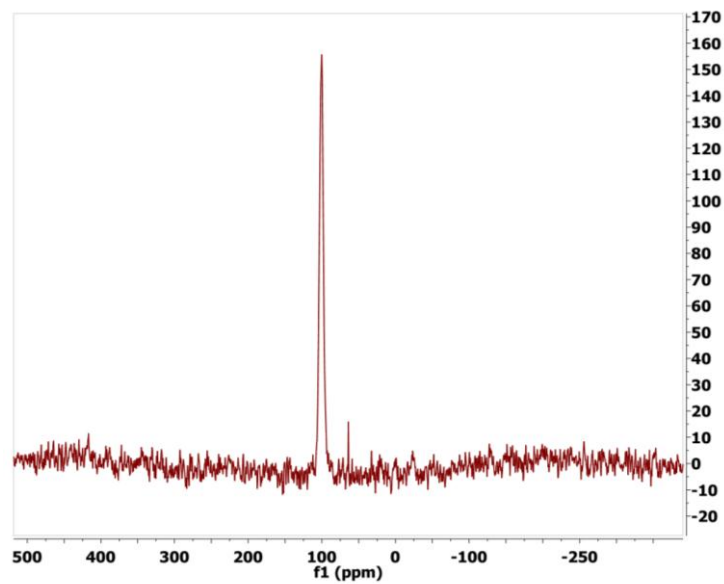


Figure S11: ^{31}P -spectrum of COP_1^{++} .

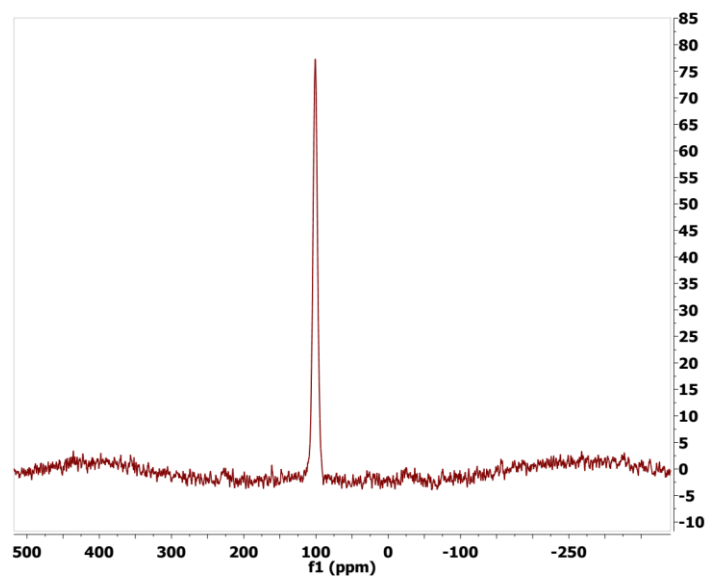


Figure S12: ^{31}P -spectrum of COP_2^{++} .

S6: PXRD analyses of polymers in their different oxidation states.

The amorphous character of polymers were determined by PXRD (Figures S13 and S14)

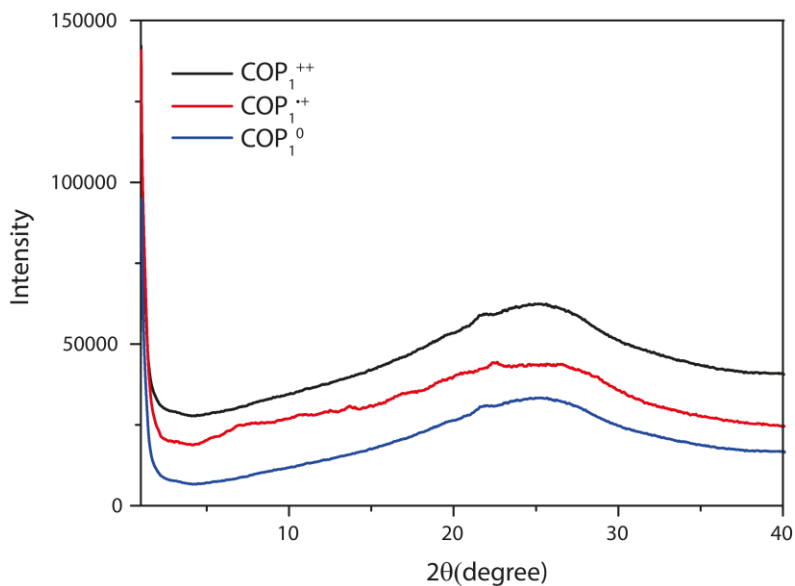


Figure S13: PXRD patterns of COP₁⁺⁺ (black), COP₁^{•+} (red) and COP₁⁰ (blue).

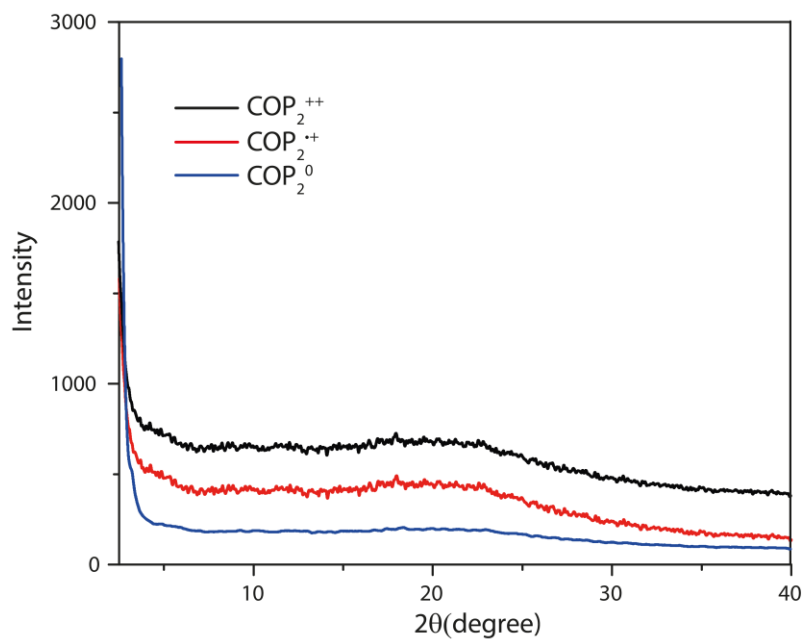


Figure S14: PXRD patterns of COP₂⁺⁺ (black), COP₂^{•+} (red) and COP₂⁰ (blue)

S7: Stability test of the polymers in ethanol.

To assess stability, the polymers were immersed in ethanol for five days and analyzed by PXRD (Figures S15, S16, S43, and S44), SEM (Figures S17, and S45), and TGA, all of which demonstrated that the polymers were robust and did not collapse upon ethanol treatment.

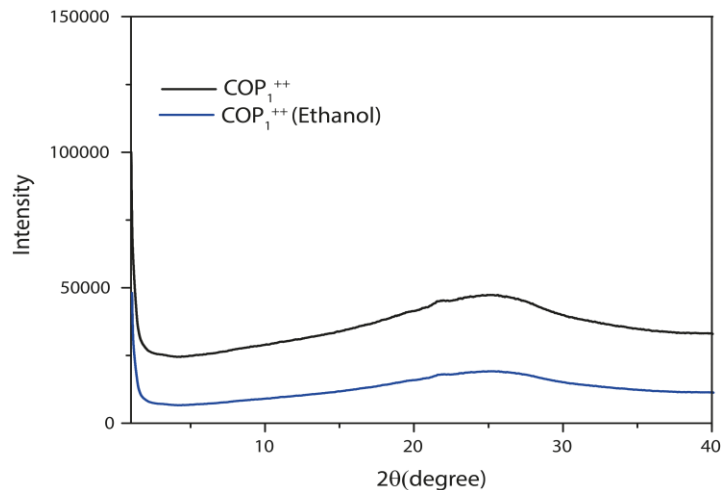


Figure S15: PXRD patterns of COP₁⁺⁺ (black), COP₁⁺⁺ after ethanol washes (blue).

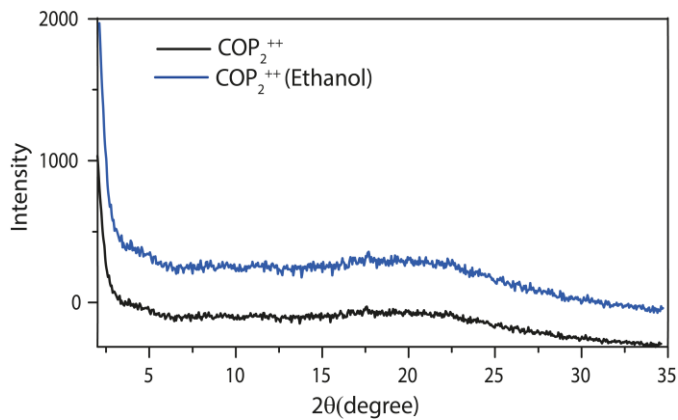


Figure S16: PXRD patterns of COP₂⁺⁺ (blue), COP₂⁺⁺ after ethanol washes (black).

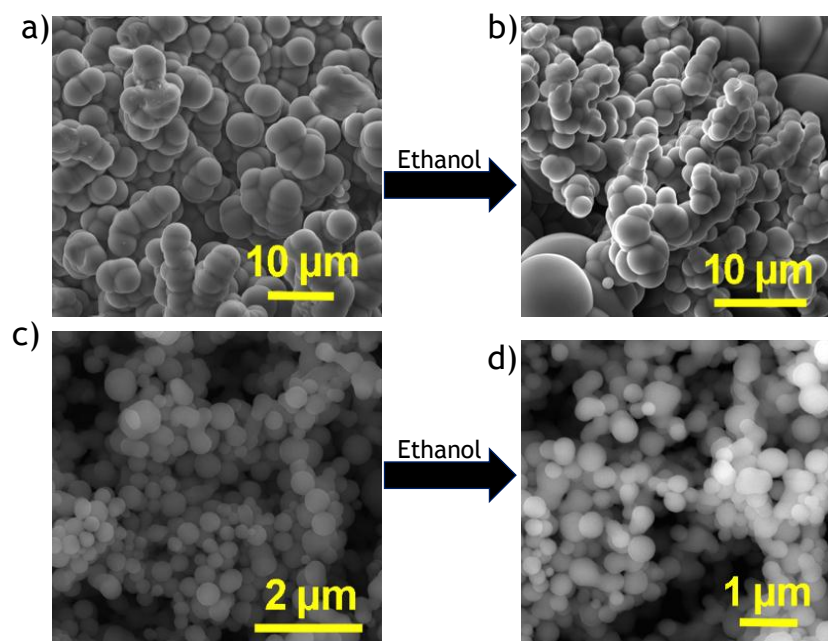


Figure S17: SEM images of COP₁⁺⁺ and COP₂⁺⁺ after ethanol wash.

S8: HRTEM images of the polymers COP₁⁺⁺ and COP₂⁺⁺.

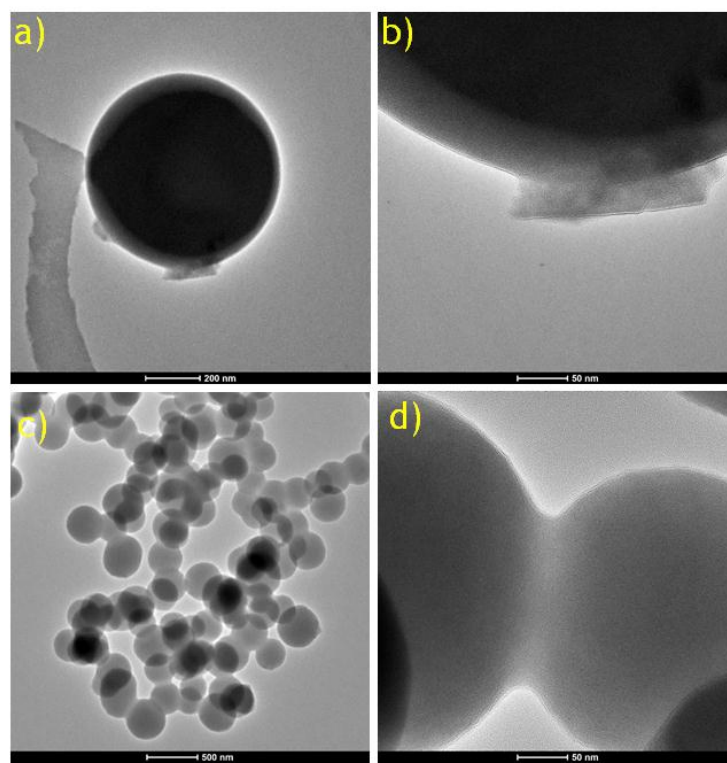


Figure S18: HRTEM images of a, b) COP₁⁺⁺ and c, d) COP₂⁺⁺.

S9: Solid-state EPR analyses of COP_2^{++} , $\text{COP}_2^{\bullet+}$ and COP_2^0 .

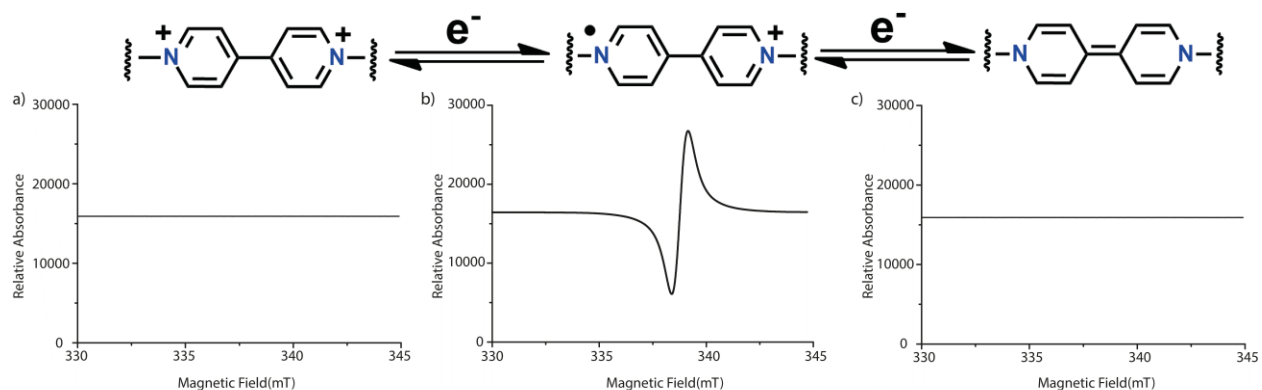


Figure S19: Solid-state EPR spectra of COP_2^{++} (a), $\text{COP}_2^{\bullet+}$ (b) and COP_2^0 (c).

S10: Radical stability of polymer $\text{COP}_1^{\bullet+}$ over time. The stability was checked by leaving the reduced powder at ambient conditions.

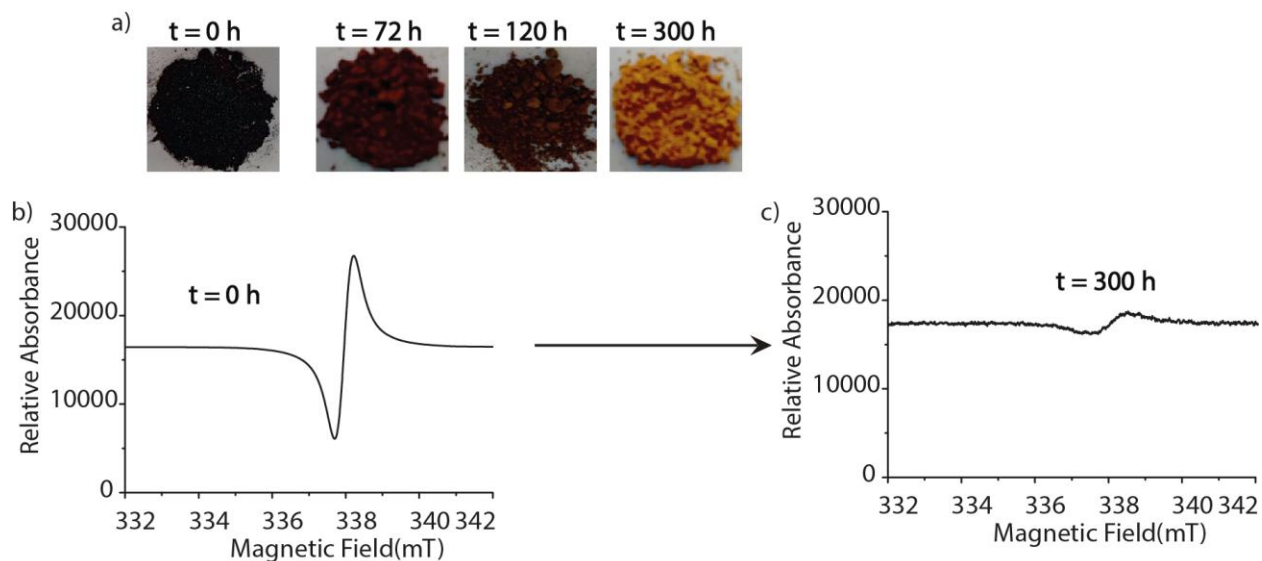


Figure S20: Color change of the polymers vs time (a), and solid-state EPR spectra of $\text{COP}_1^{\bullet+}$ over 300 h (b).

S11: SEM analysis after exposure to sunlight

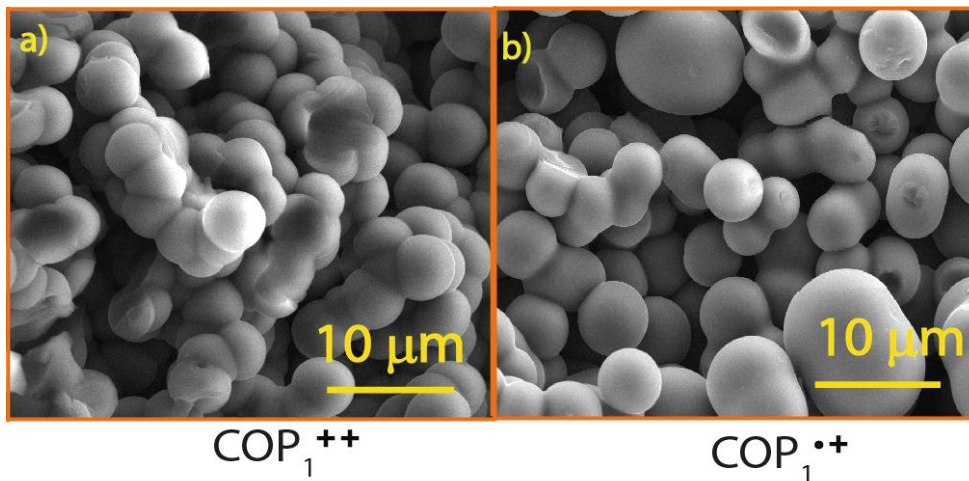


Figure S21: SEM images of COP₁⁺⁺ (a) and COP₁^{*+} (b).

S12: Solid-state UV-Vis spectroscopic measurements for all the polymers

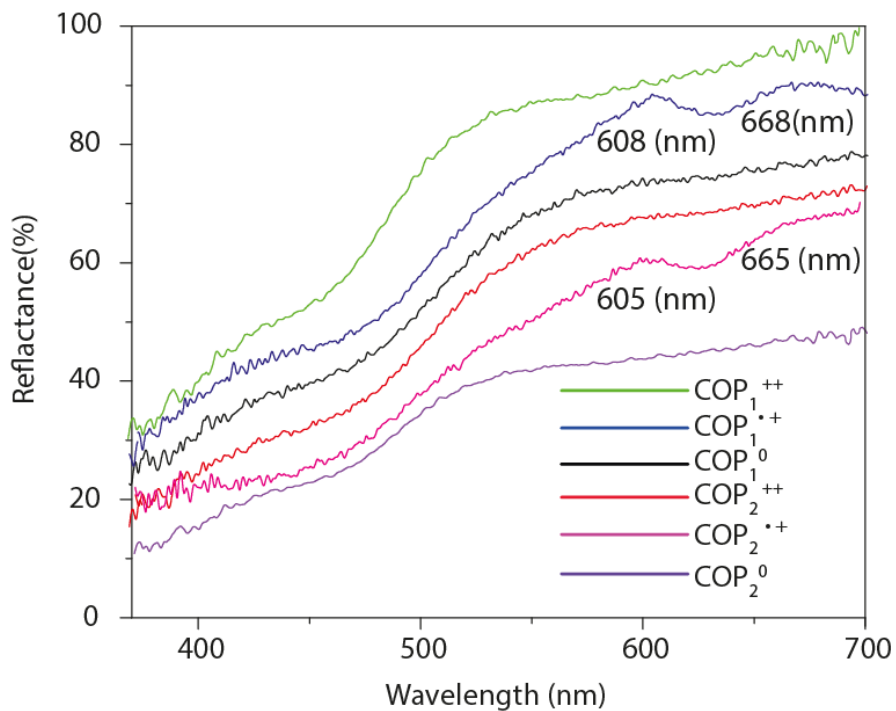


Figure S22: Solid-state UV-Vis spectra of COP₁⁺⁺ (green), COP₁^{*+} (blue), COP₁⁰ (black) and COP₂⁺⁺ (red), COP₂^{*+} (Pink), COP₂⁰ (Violet).

S13: Stability of the polymers during ammonia detection

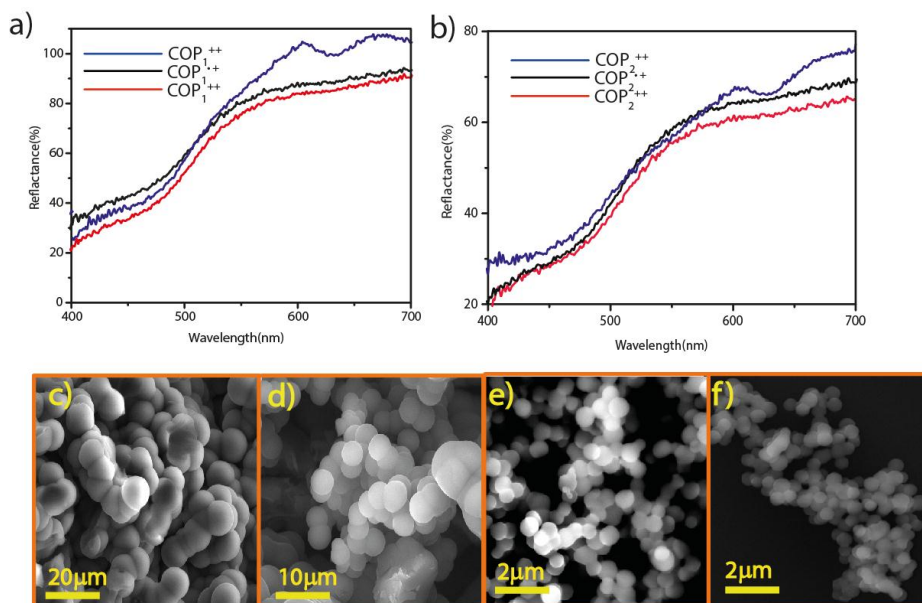


Figure S23: Solid-state UV-Vis spectra of a) COP₁⁺⁺, COP₁¹⁺ and COP₁⁰ and b) COP₂⁺⁺, COP₂¹⁺ and COP₂⁰.

SEM images of COP₁⁺⁺ (c) COP₁¹⁺ (d), COP₂⁺⁺ (e) and COP₂¹⁺ (f).

S14: Nitrogen (N₂) and carbon dioxide (CO₂) adsorption studies for COP₁⁺⁺ and COP₂⁺⁺ at room temperature and at 77K

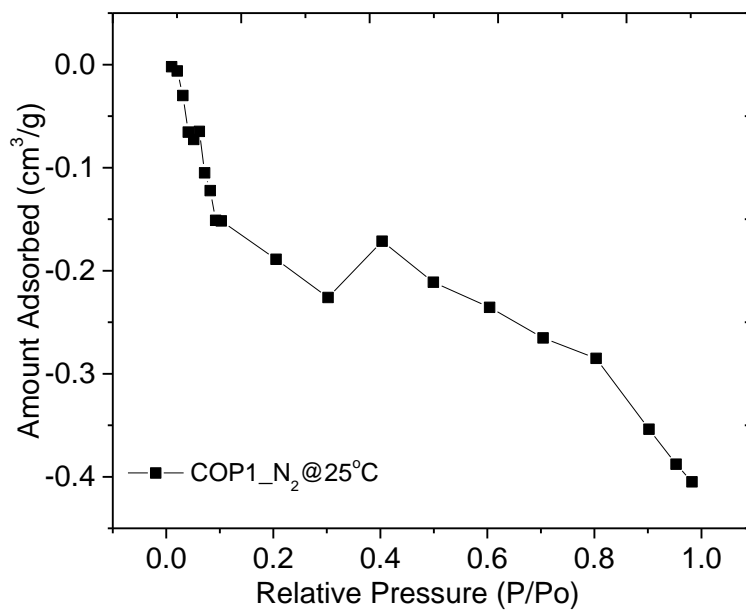


Figure S24: N₂ adsorption isotherm of COP₁⁺⁺ at room temperature.

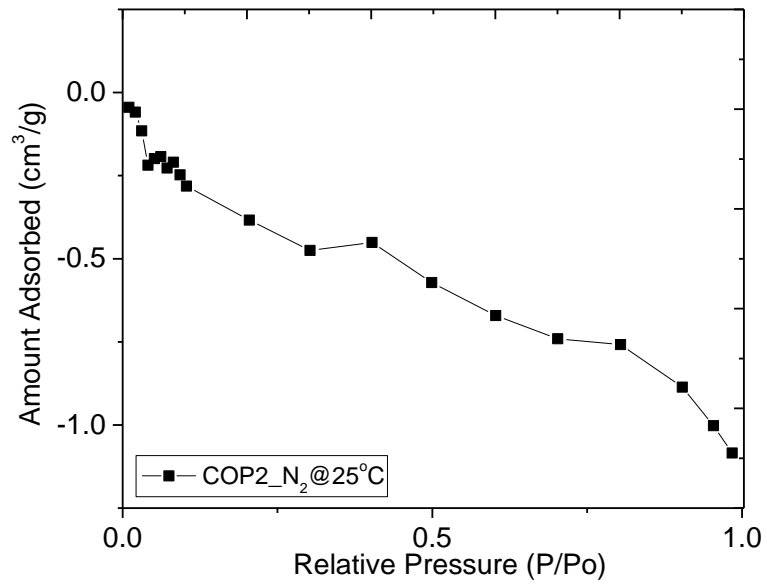


Figure S25: N₂ adsorption isotherm of COP₂⁺⁺ at room temperature.

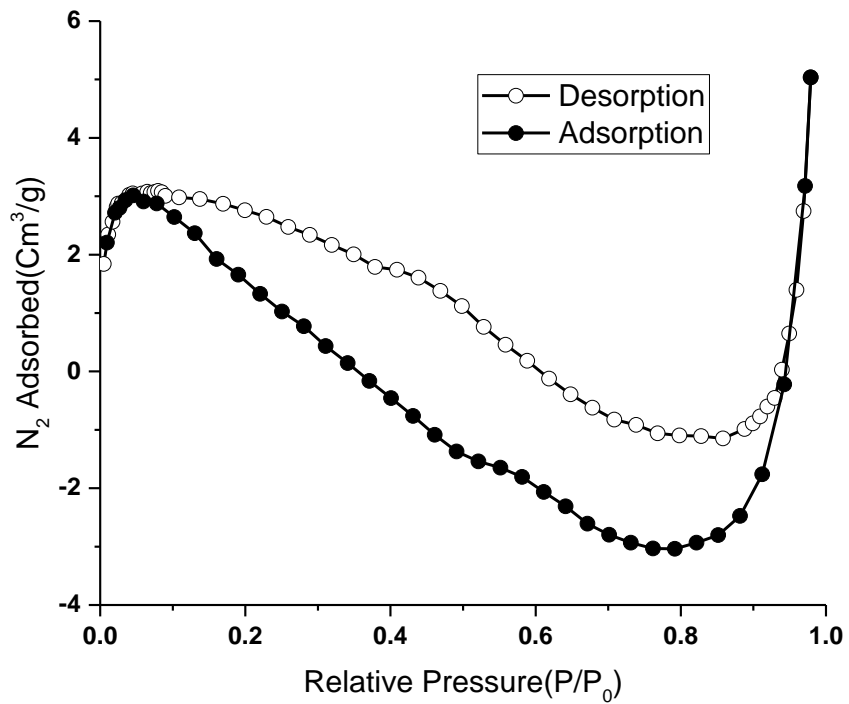


Figure S26: N₂ adsorption isotherm of COP₁⁰ at 77K.

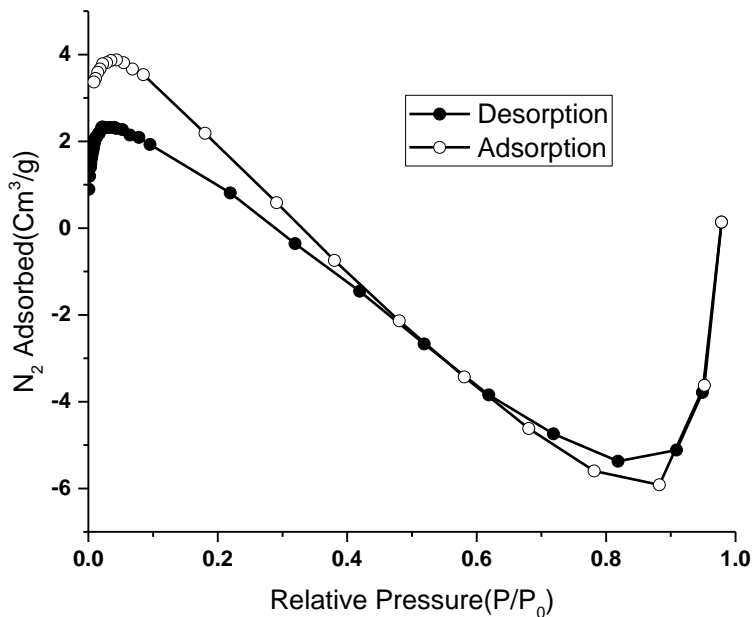
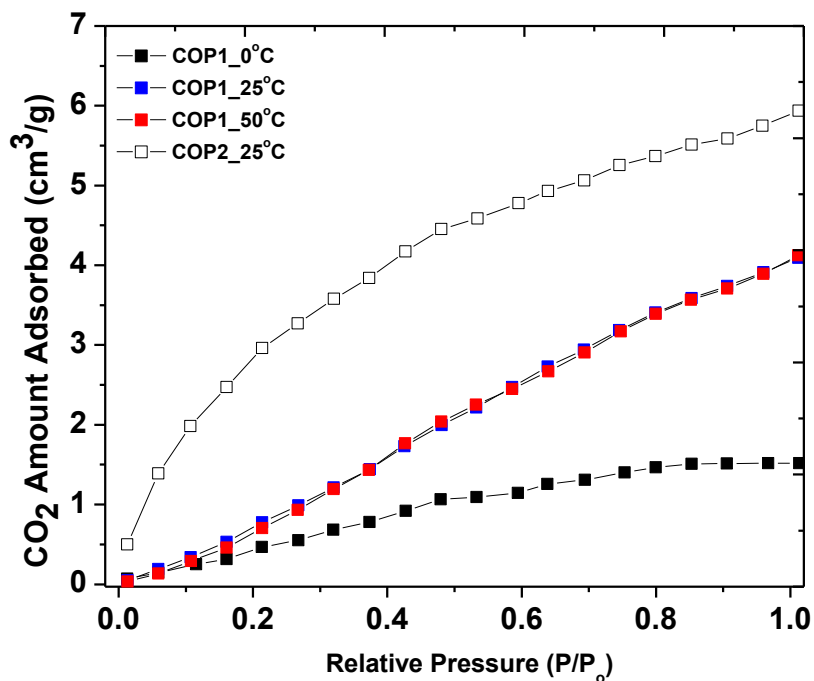


Figure S27: N₂ adsorption isotherm of COP₂⁰ at 77K.



FigS28: CO₂ adsorption isotherms for COP₁⁺⁺ and COP₂⁺⁺ at various temperature near ambient conditions.

CO₂ has a significant quadrupole moment (-1.4×10^{35} Cm) that leads to specific interactions with the adsorbents (molecular orientation, hydrogen bonding...) and given the non-porous nature of the specific

adsorbents, it can be stated that the CO₂ adsorption is induced based on these interactions. Both COPs synthesized herein present tertiary nitrogen atoms in their structures that play crucial role in the reversible CO₂ binding. The CO₂ adsorption on the COP₁⁺⁺ at 0 °C follows a very different profile (step-wise) than the one at 25 and 50 °C (almost linear increase), respectively. In the case of 25 and 50 °C, the CO₂ adsorption capacity reaches 4 cm³/g at 1 bar. In the case of COP₂⁺⁺ at 25 °C, a steeper rise of CO₂ uptake at lower pressures can be noticed from the isotherm, reaching a maximum of 6 cm³/g at 1 bar. Comparatively, the N₂ uptake at 25 °C is almost zero. The CO₂-COP⁺⁺ interaction a promising indicator for Lewis basic sites in the materials under study. However, the low porosity of the COPs limits the accessibility of the Lewis basic sites and thus leads to somehow not high values of CO₂ adsorption capacity. We also, calculated the isosteric heat of adsorption (Q_{st}) for the CO₂ adsorption over COP1. At the onset of adsorption was found to be 10.9 kJ/mol. This value is substantially lower than 45 kJ/mol that has been reported for amino-functionalized MOF materials. This moderately low adsorption affinity for CO₂ could be due to the absence of porosity, which rather limits the Lewis basic sites accessibility. We also recorded the nitrogen adsorption of the polymers in their neutral state at 77K.

S15: UV-Vis spectra iodine in cyclohexane solutions of known concentrations. The maximum of absorbance ($\lambda_{\text{max}} = 526 \text{ nm}$) was plotted against the concentration of iodine to generate the calibration curve shown in the Figure S24. The calibration curve was used to determine the efficiency of removal of I₂ for a solute by the polymers.

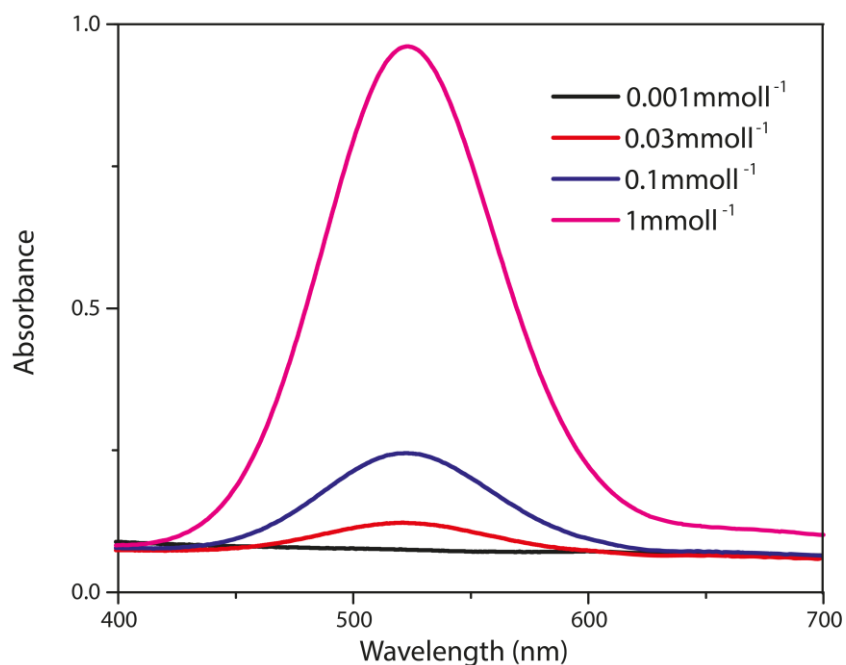


Figure S29: UV-Vis spectra of I₂ in cyclohexane at different concentrations recorded at room temperature.

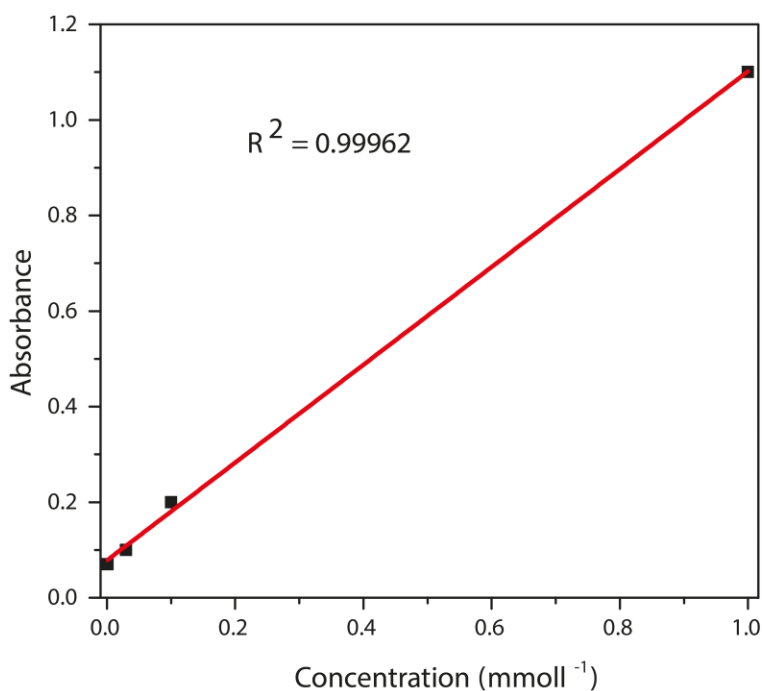


Figure S30: Calibration curve of iodine obtained from UV-Vis spectra.

S16: Time-dependent removal efficiency of iodine

The efficiency of iodine removal (in %) by the sorbent from solution (cyclohexane) was determined by the following equation:

Removal efficiency (%) = $(C_0 - C)/C_0 \times 100$, where C_0 and C are the initial and final concentrations after complete adsorption of iodine. The concentrations of iodine in stock solutions as well as in the filtrates were characterized by UV-Vis spectroscopy. All experiments were carried out at room temperature, in cyclohexane.

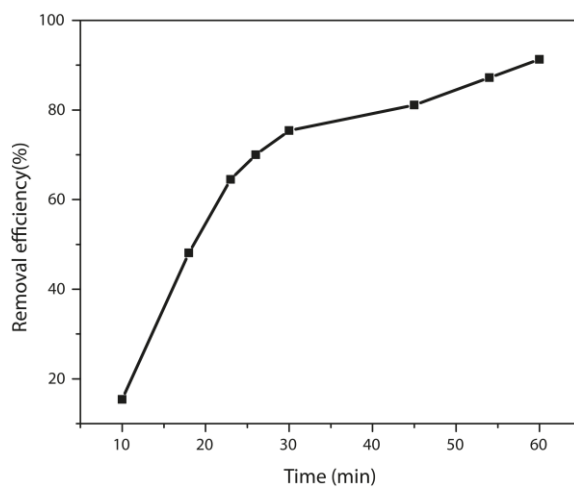


Figure S31: Removal efficiency of iodine by COP_1^{++} .

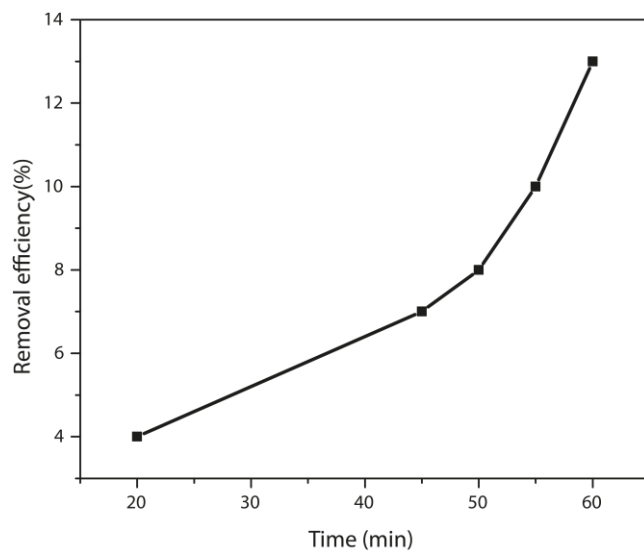


Figure S32: Removal efficiency of iodine by COP_1^{*+} .

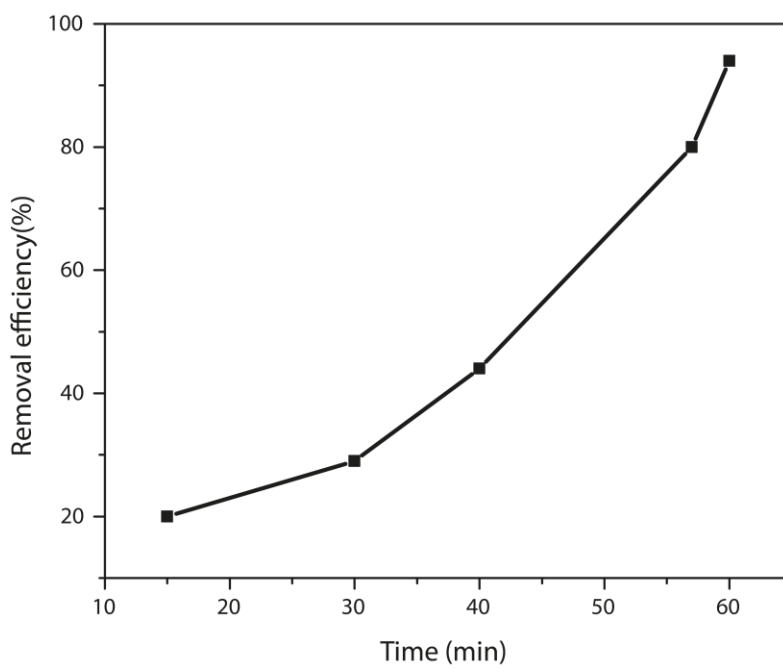


Figure S33: Removal efficiency of iodine by COP_1^0 .

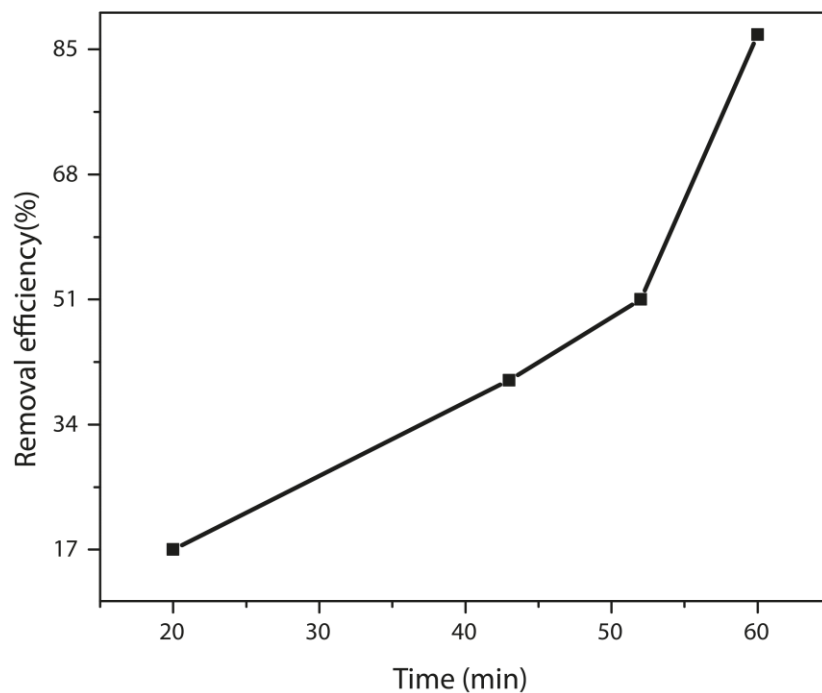


Figure S34: Removal efficiency of iodine by COP_2^{++} .

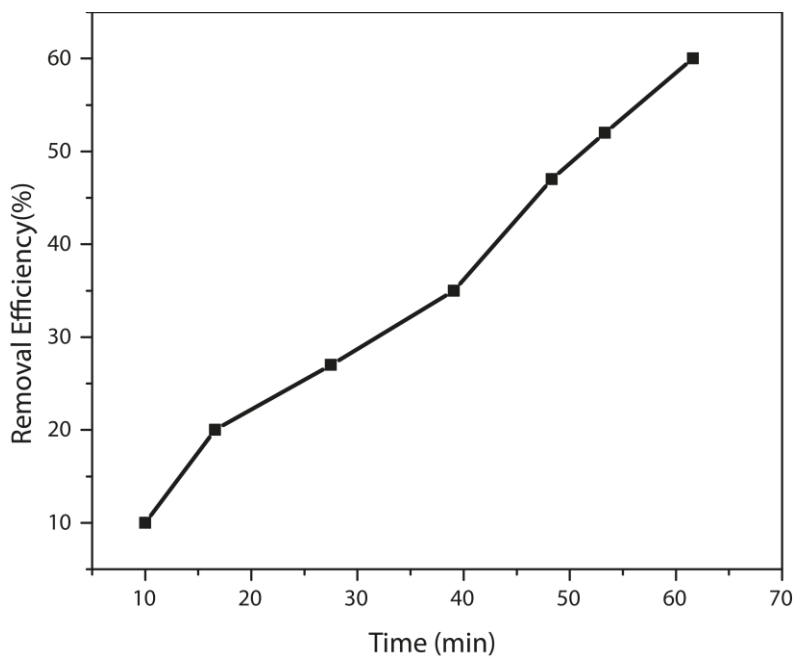


Figure S35: Iodine removal efficiency by COP_2^{*+} .

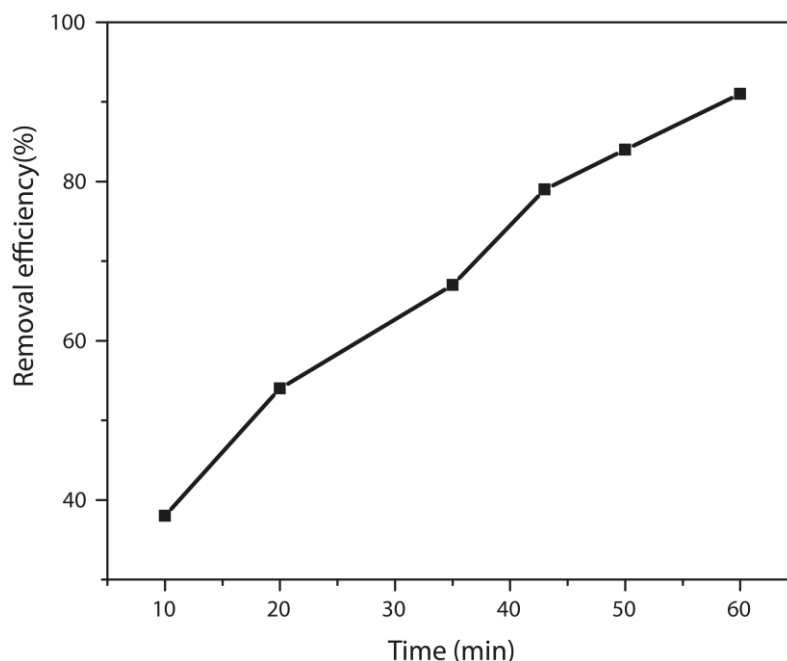


Figure S36: Iodine removal efficiency by COP_2^0 .

S17: Theoretical study of polymers to understand the mechanism for iodine and ammonia capture.
Computational details

Full geometry optimizations of model compound M_2^{++} and the $\text{M}_2^{+++}\text{I}_2$, $\text{M}_2^{+++}(\text{I})_2$ and $\text{M}_2^{+++}(\text{I}_3)$ systems were performed using DFT within the hybrid meta-GGA approximation with the M06 functional and the Gaussian 09 package (Revision D.01).³ The standard 6 311G(d,p)⁴ basis set was used throughout. No symmetry constraints have been imposed during the optimizations. The stationary points found on the potential energy surfaces as a result of geometry optimizations were tested to represent energy minima rather than saddle points via frequency analysis. The default values for the integration grid (75 radial shells and 302 angular points) and the SCF energy convergence criteria (10^{-8}) were used in all calculations. The calculated binding energies include corrections for basis set superposition errors (BSSEs), which were calculated using the standard Counterpoise method.⁵

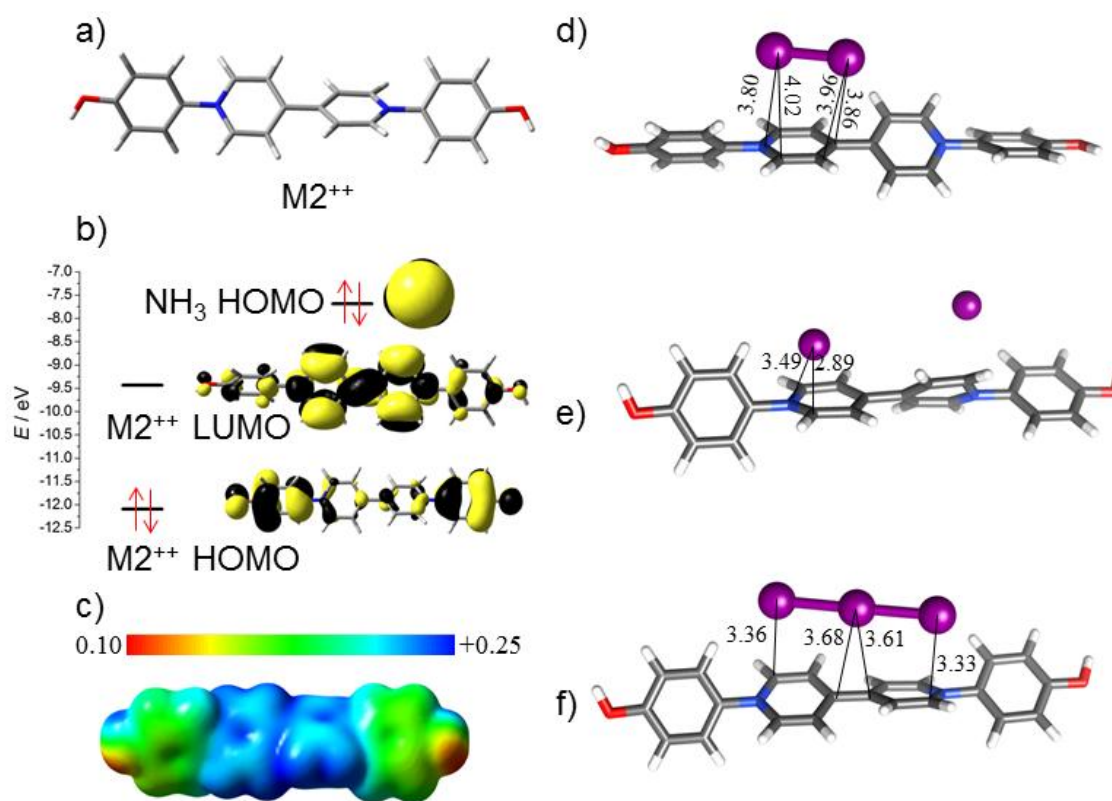


Figure S37: Structure of the M2++ model system (a), isodensity contours of the HOMO and LUMO of M2++ and the HOMO of NH3, electrostatic potential (a. u.) on the surface of M12+ (c), and optimized geometries of, M12+•I2 (d), M1+++•(I-)2 (e) and M2++•(I3) (f). Distances are given in Å. All calculations were performed at the M06/6 311G(d,p) level.

S18: Solid state Raman spectral analysis of all the iodine loaded Polymers

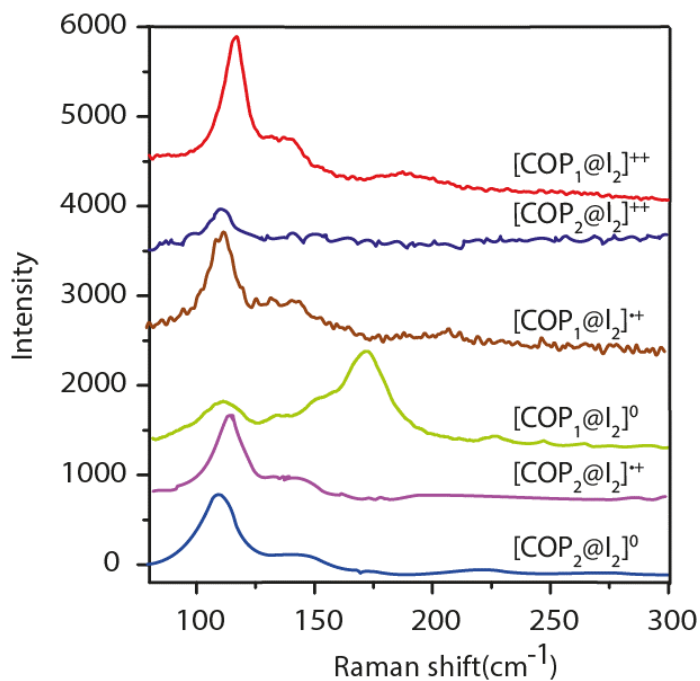


Figure S38: Raman spectra of iodine loaded COP⁺⁺, COP⁺ and COP⁰.

S19: Solid state XPS analysis of all iodine loaded Polymers

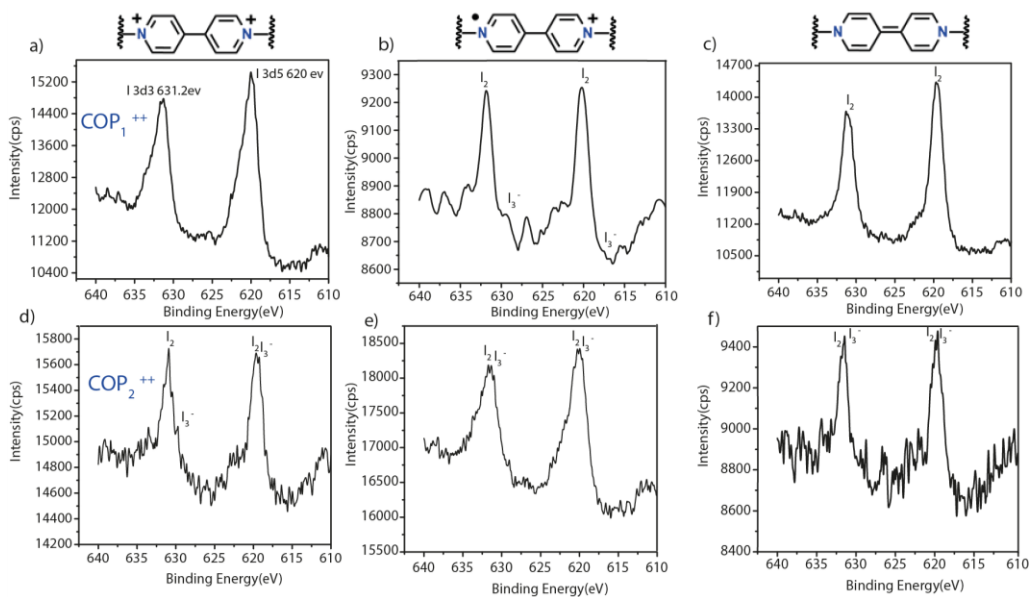


Figure S39: XPS spectra of iodine loaded COP⁺⁺, COP⁺ and COP⁰.

Table S20: Comparison of Iodine capture with other reported materials.

Sample	Iodine sorption method	Time taken for I ₂ adsorption	Temperature (K)	Iodine uptake (wt %)	Ref.
PAF-1	Fixed vapor pressure	10 h (In n-hexane)	333	74.2	<i>J. Mater. Chem. A</i> , 2014, 2 , 7179-7187
JUC-Z2	Vacuum swing adsorption	10 h (In n-hexane)	298	59.0	<i>J. Mater. Chem. A</i> , 2014, 2 , 7179-7187
JUC-Z2	Fixed vapor pressure	10 h (In n-hexane)	333	80.4	<i>J. Mater. Chem. A</i> , 2014, 2 , 7179-7187
{[Zn ₃ (DLlac) ₂ (pybz) ₂] _n ·2.5DMF} _n	Vapor adsorption/Cyclohexane	90min(Vapor) 48h(Cyclohexane)	-	82.6	<i>J. Am. Chem. Soc.</i> 2010, 132 , 2561–2563
PAF-23	Vapor adsorption/Cyclohexane	48h(Vapor) 72h (cyclohexane)	348	271	<i>Angew. Chem. Int. Ed.</i> 2015, 54 , 12733–12737
PAF-24	Vapor adsorption/Cyclohexane	48h(Vapor) 72h (cyclohexane)	348	276	<i>Angew. Chem. Int. Ed.</i> 2015, 54 , 12733–12737
PAF-25	Vapor adsorption/Cyclohexane	48h(Vapor) 72h (cyclohexane)	348	260	<i>Angew. Chem. Int. Ed.</i> 2015, 54 , 12733–12737
Azo-Trip	Vapor adsorption/Cyclohexane	48h (Vapor) 36h(cyclohexane)	350	233	<i>Polym. Chem.</i> , 2016, 7 , 643–647
NiP-CMP	Vapor adsorption/Cyclohexane	48h (Vapor) 24h (cyclohexane)	350	202	<i>Chem. Commun.</i> , 2014, 50 , 8495-8498
[Mo ₃ S ₁₃]	Vapor	24 h	333	100	<i>J. Am. Chem. Soc.</i> 2015, 137 , 13943–13948
Sb ₄ Sn ₃ S ₁₂ , Zn ₂ Sn ₂ S ₆ , and K _{0.16} CoS _x	Vapor	48h	348	225	<i>Chem. Mater.</i> 2015, 27 , 2619–2626
(BEA) ₂ [PbBr ₄]	Vapor	4-72h	313	43	<i>Angew. Chem. Int. Ed.</i> 2014, 53 , 1039–1042
COP ₁ ⁺⁺	Vapor/Cyclohexane	3min (Vapor)	333	212	This Work
COP ₁ ^{•+}	Vapor/Cyclohexane	3min (Vapor)	333	195	This Work
COP ₁ ⁰	Vapor/Cyclohexane	3min (Vapor)	333	380	This Work
COP ₂ ⁺⁺	Vapor/Cyclohexane	3min (Vapor)	333	258	This Work
COP ₂ ^{•+}	Vapor/Cyclohexane	3min (Vapor)	333	211	This Work
COP ₂ ⁰	Vapor/Cyclohexane	3min (Vapor)	333	277	This Work

N.B: Equilibrium uptake in weight (%) $\alpha = (m_2 - m_1)/m_1 \times 100$ wt%, m_1 = Sample mass and m_2 = (Sample + iodine) mass.

S21: Energy-dispersive X-ray spectroscopy study

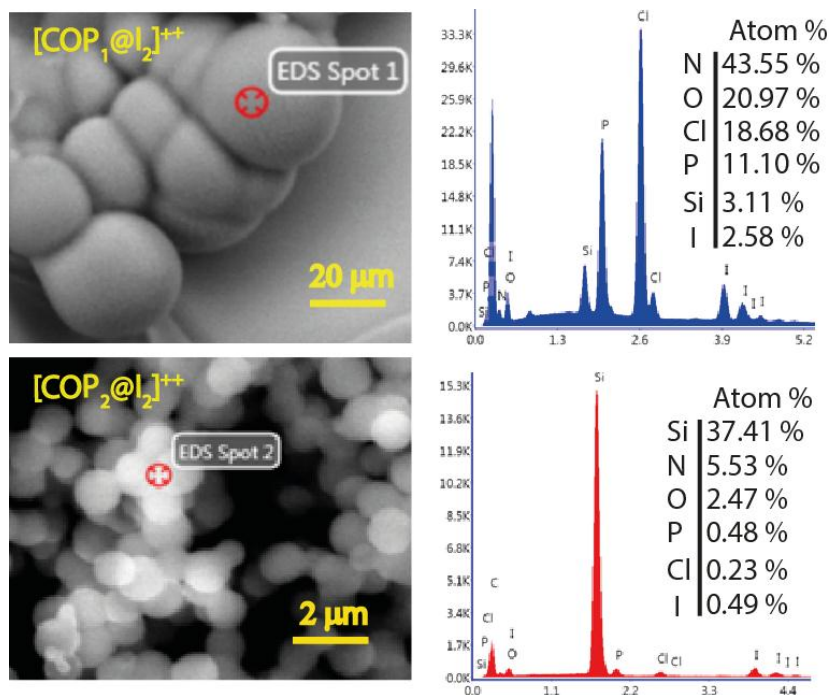


Figure S40: EDS spectra of [COP₁@I₂]⁺⁺ and [COP₂@I₂]⁺⁺ confirm the presence of iodine within the polymers.

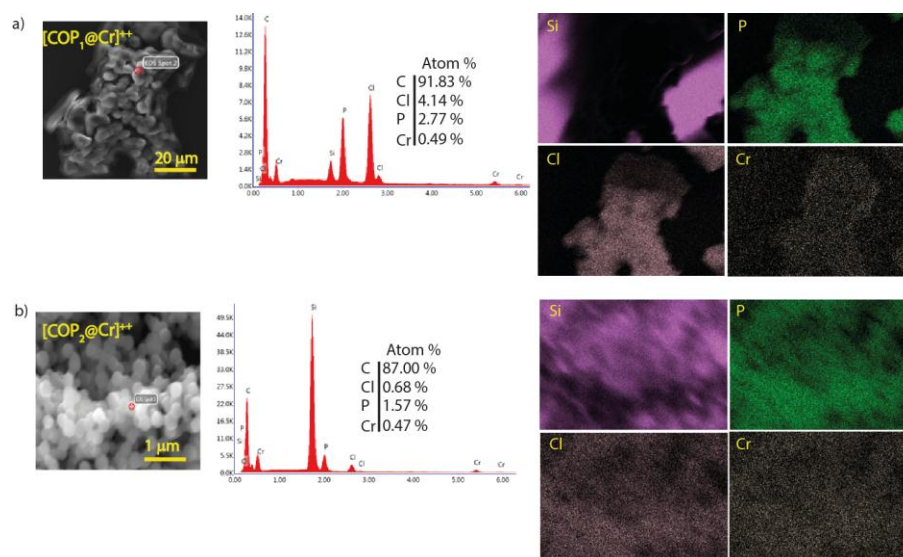


Figure S41: EDS spectra of [COP₁@Cr]⁺⁺ and [COP₂@Cr]⁺⁺ confirm the presence of dichromate within the polymers.

S22: Characterization of the two polymers after iodine removal

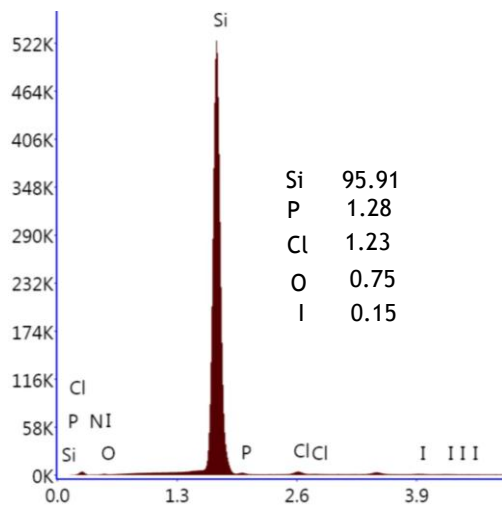


Figure S42: EDX spectra of COP_1^{++} after the removal of iodine.

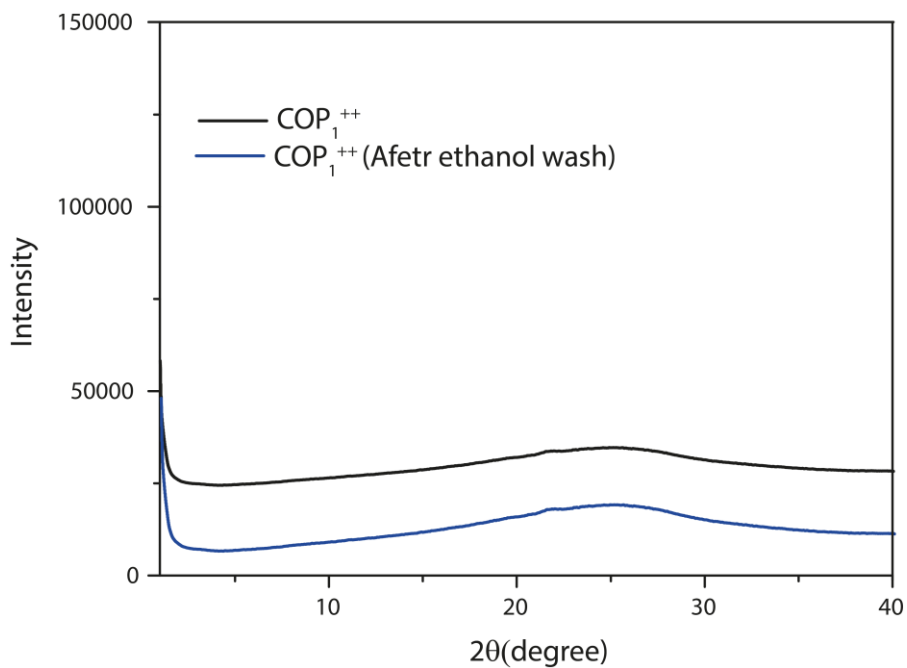


Figure S43: PXRD profile of COP_1^{++} after the removal of iodine.

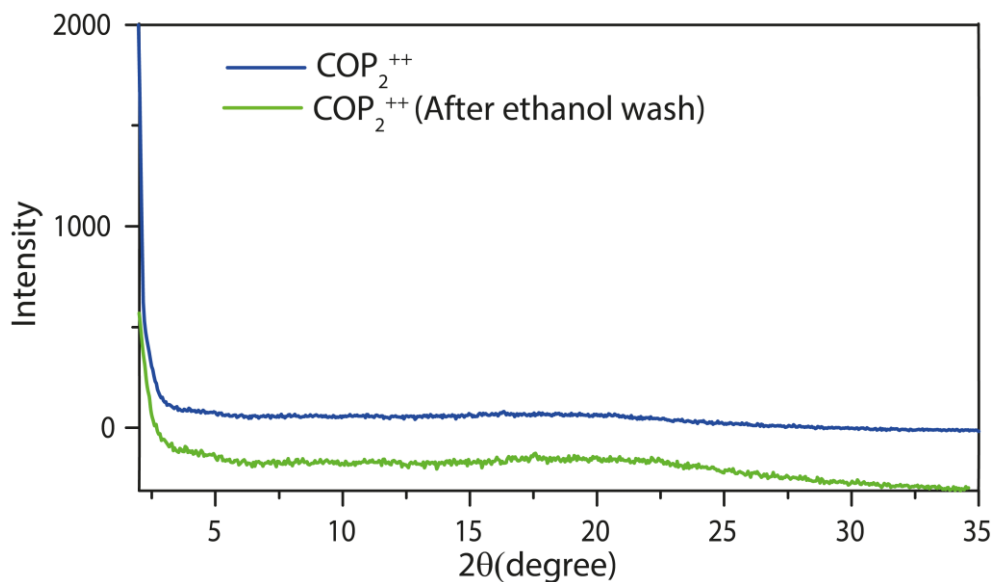


Figure S44: PXRD profile of COP₂⁺⁺ after the removal of iodine.

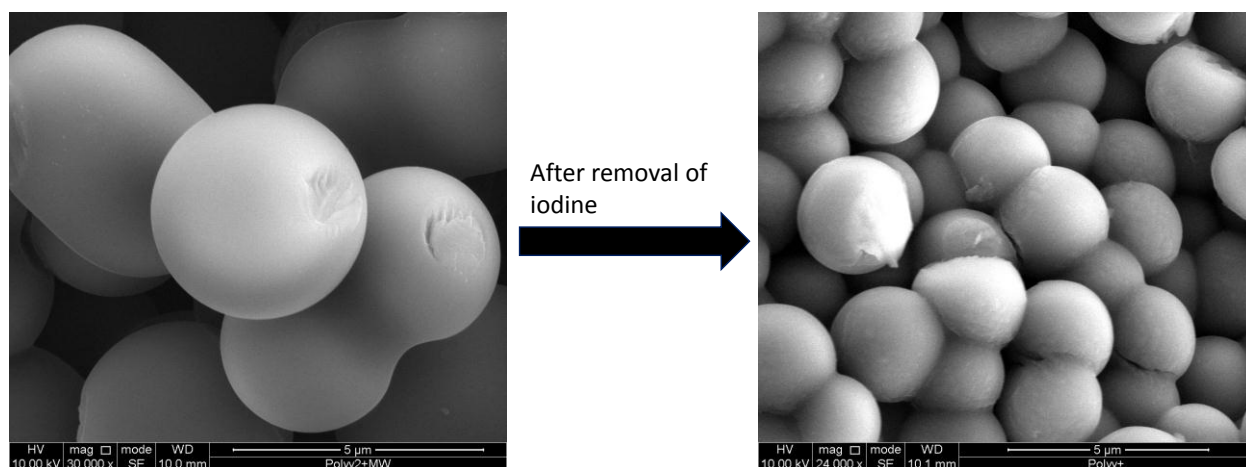


Figure S45: SEM images of COP₂⁺⁺ before (left) and after (right) removal of iodine by ethanol washings.

S23: Reusability study of the polymers after iodine and dichromate removal.

The reusability of the polymer was carried out by dissolving 15 mg of iodine-loaded polymer in ethanol and washed several times and dried at 60 °C in vacuum oven, and reused for the iodine adsorption from cyclohexane and monitored by UV-Vis spectroscopy. Similarly, dichromate loaded polymer was reused by dissolving 15 mg of loaded polymer in saturated solution of NaCl and washed several time and dried at 60 °C in vacuum oven and subsequently, the UV-Vis measurement was repeated at different time intervals. For each cycle, the experiment was carried out three times.

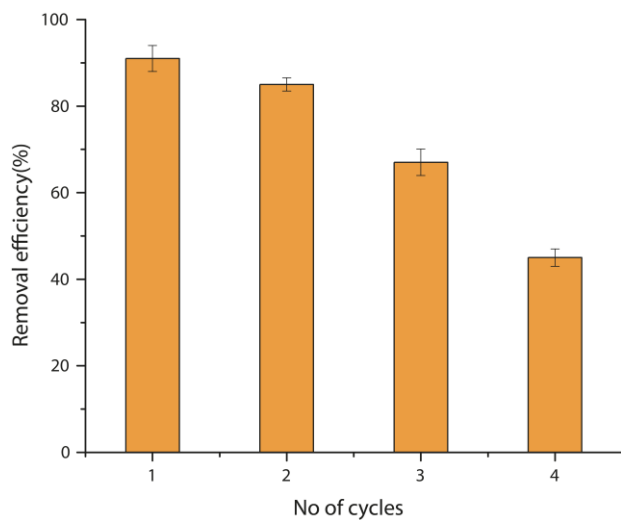


Figure S46: Reusability of COP_1^{++} for iodine adsorption.

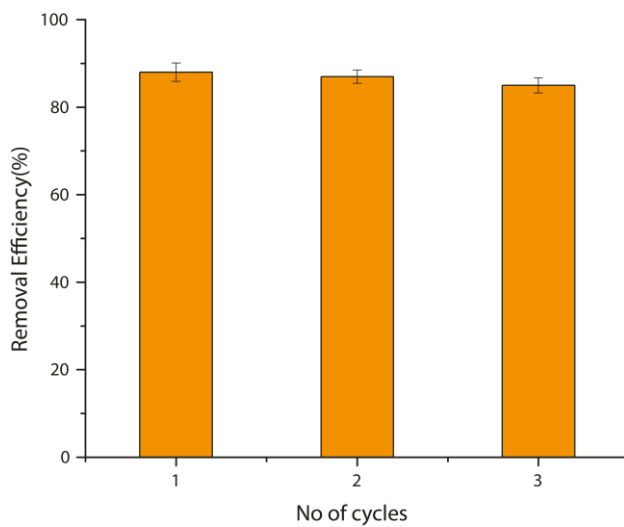


Figure S47: Reusability of COP_1^{++} for $\text{Cr}_2\text{O}_7^{2-}$ adsorption in solid state.

References:

1. Cil, E. *Inorg. Chim. Acta* **2009**, 362, 1421.
2. J. Barbera, J. Jimenez, A. Laguna, L. Oriol, S. Perez, and J. L. Serrano, *Chem. Mater.*, 18, **2006**, 5439.
3. Zhao, Y.; Truhlar, D. G. *Theor. Chem. Account* **2008**, 120, 215-241.

4. Gaussian 09, Revision D.01, Frisch, M. J.; Trucks, G. W.; Schlegel, H. B.; Scuseria, G. E.; Robb, M. A.; Cheeseman, J. R.; Scalmani, G.; Barone, V.; Mennucci, B.; Petersson, G. A.; Nakatsuji, H.; Caricato, M.; Li, X.; Hratchian, H. P.; Izmaylov, A. F.; Bloino, J.; Zheng, G.; Sonnenberg, J. L.; Hada, M.; Ehara, M.; Toyota, K.; Fukuda, R.; Hasegawa, J.; Ishida, M.; Nakajima, T.; Honda, Y.; Kitao, O.; Nakai, H.; Vreven, T.; Montgomery, Jr., J. A.; Peralta, J. E.; Ogliaro, F.; Bearpark, M.; Heyd, J. J.; Brothers, E.; Kudin, K. N.; Staroverov, V. N.; Kobayashi, R.; Normand, J.; Raghavachari, K.; Rendell, A.; Burant, J. C.; Iyengar, S. S.; Tomasi, J.; Cossi, M.; Rega, N.; Millam, N. J.; Klene, M.; Knox, J. E.; Cross, J. B.; Bakken, V.; Adamo, C.; Jaramillo, J.; Gomperts, R.; Stratmann, R. E.; Yazyev, O.; Austin, A. J.; Cammi, R.; Pomelli, C.; Ochterski, J. W.; Martin, R. L.; Morokuma, K.; Zakrzewski, V. G.; Voth, G. A.; Salvador, P.; Dannenberg, J. J.; Dapprich, S.; Daniels, A. D.; Farkas, Ö.; Foresman, J. B.; Ortiz, J. V.; Cioslowski, J.; Fox, D. J. Gaussian, Inc., Wallingford CT, **2009**. Hay, P. J.; Wadt, W. R. *J. Chem. Phys.* **1985**, *82*, 270.
5. Bernardi, F.; Boys, S. F. *Mol. Phys.* **1970**, *19*, 553-566.